NASA-CR-192127

RESEARCH IN ROBUST CONTROL FOR HYPERSONIC VEHICLES

Progress Report #1
November 1992

1 July 1992 - 30 November 1992

Research supported by the NASA Langley Research Center
NASA Grant Number: NAG-1-1451

Principal Investigator: A.J. Calise
Research Assistant: H. Buschek
NASA Grant Monitors: J.D. McMinn
I. Gregory

School of Aerospace Engineering
Georgia Institute of Technology
Atlanta, Georgia 30332

Summary

During the first reporting period research has concentrated on finishing the modeling work required for a representative model of a scramjet propulsion system for hypersonic vehicles. An existing hypersonic propulsion code has been adjusted to the Winged-Cone Configuration used in this study. In this process the complete force and moment calculation has been revised. The advantageous feature of the code to account for angle of attack variations was then used to compute the thrust, lift and pitching moment contributions of the propulsion system not only for various Mach numbers and fuel equivalence ratios, but also for different angles of attack.

1 Introduction

The objective of this research is to address the issues associated with the design of robust integrated flight control systems for future hypersonic vehicles with airbreathing propulsion systems. It is anticipated that such vehicles will exhibit significant interactions between rigid body (airframe) dynamics, structural dynamics and engine dynamics. The uncertainty in the initial dynamic models developed for these vehicles will also be high. The main reason that highly interactive uncertain dynamics are to be expected is that scramjet engines will be the primary source of propulsion at hypervelocity speeds. Wind-tunnel testing as a result will be limited, and it will be necessary to gain experience in actual flight testing of such vehicles. This means that initial flight control system design efforts will rely more heavily on theoretical and computer based models, than has been the case for subsonic and supersonic aircraft. Also, propulsion system sensitivity to angle of attack variations will lead to highly interactive dynamics.

In this study, the current major research issues from a flight control viewpoint are: (1) the development of models that are representative of the interactive dynamics that can occur in such vehicles, (2) the development of representative uncertainty models for these dynamics and (3) the development of practical approaches to designing multivariable flight control systems that guarantee adequate performance in the presence of uncertainty. The research done during the first reporting period has been focussing on item (1).

The hypersonic vehicle model described in [1] neglects the effects of angle of attack variations on propulsion system performance. For long, slender bodies with a considerable amount of the compression of the flow going through the engine taking place on the forebody, this assumption may not necessarily be valid for the entire flight regime. Flying under an angle of attack, an axisymmetric vehicle with engine modules 'wrapped' all around the body experiences greater compression on the underside than on the upperside. This results in changes in thrust vector magnitude and direction and therefore in flight behavior of the vehicle.

To investigate the angle of attack sensitivity of the propulsion system and the impact on vehicle performance the HYTHRUST code described in [2] is used. The code as it is presently employed evaluates the thrust, lift, and pitching moment contribution of a propulsion unit for various Mach numbers, equivalence ratios, and angles of attack. The thrust specific impulse is also computed.

2 Current Research Results

2.1 Vehicle Description

As mentioned above, the Winged-Cone Configuration described in [1] is used in this study. Main characteristics of this vehicle are an axisymmetric conical forebody, a cylindrical engine nacelle section with engine modules all around the body, and a cone frustrum engine nozzle section.

The size of an individual engine module was based on information from an input file for the 'SRGULL' program (courtesy of J.D. McMinn, NASA LaRC) and have been modified in order to meet certain requirements. These modifications consisted of reducing the wedge angle in the inlet in order to avoid subsonic flow inside the scramjet engine at low Mach numbers, and reducing the height of an engine module to prevent the bowshock from entering the inlet at high Mach numbers and angles of attack. Also, the outer shape was somewhat simplified to achieve a better implementation into the code (e.g. the streamtubes as they are currently defined do not account for expansion in a vertical direction, so this kind of shape was avoided). According to the given width of the inlet a total of 32 modules are attached to the vehicle. One of the modules is shown in fig. 1.

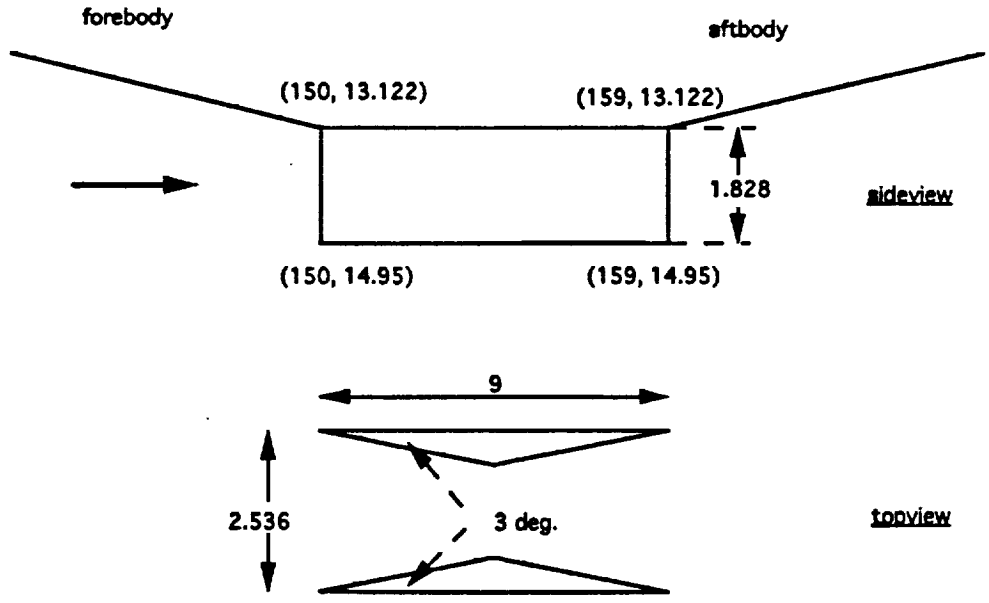

Figure 1: Engine module as used in HYTHRUST, all measurements in ft.

2.2 Determination of Forces and Moments

The calculation of the forces and moments created by the propulsion system has been revised entirely compared to the version given in [2]. In what follows, a brief outline is given describing how the relevant forces and moments are computed.

The control volume consists of (see fig. 2)

1. inlet entrance plane
2. engine surface at body
3. engine exit plane
4. engine surface at cowl
5. aftbody surface.

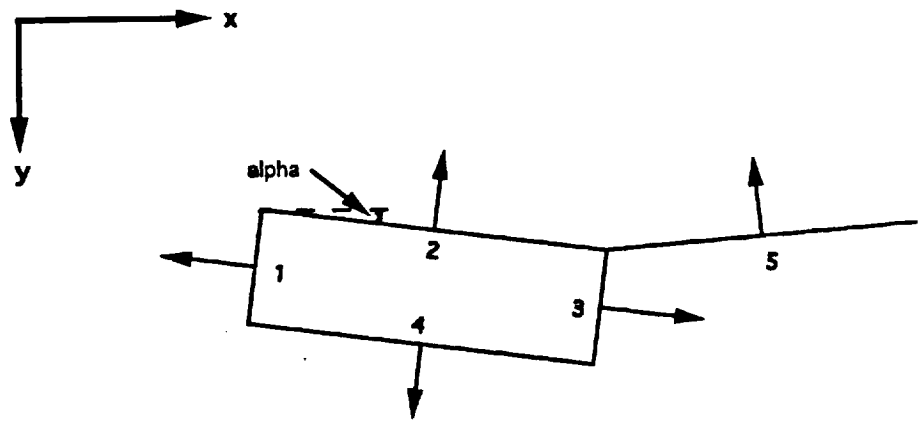

Figure 2: Control volume for force computation, vectors indicate outward normal.

The coordinate system chosen is a two-dimensional windframe system with the x-axis positive rearward, the y-axis positive downward, and the pitching moment positive nose up. This convention was chosen because the vehicle geometry is already given in this system. It is distinguished between two different types of forces: forces created by momentum flux, F_m, and forces created by pressure, F_p, both resolved in directions of the coordinates. The pitching moments caused by these forces are M_m and M_p, it is again

distinguished if they are caused by an x- or y-force (M_{xm}, M_{ym}, M_{xp}, M_{yp}).

1. Inlet Entrance Plane

Since for this configuration the streamtubes are parallel to the body x-axis the outward normal is $\vec{n}_1 = (-\cos\alpha, -\sin\alpha)$, where α is the angle of attack. The incoming flow from the forebody has the velocity $\vec{v}_1 = v_1(\cos\theta_1, \sin\theta_1)$. Using the momentum equation and the expression

$$\begin{aligned} \vec{v}_1 d\vec{A}_1 &= \vec{v}_1 \vec{n}_1 \, dA_1 \\ &= -v_1 \cos(\theta_1 - \alpha) \, dA_1 \end{aligned} \tag{1}$$

the forces caused by the momentum flux for each streamtube are

$$\begin{aligned} d\vec{F}_{m1} &= \rho \vec{v}_1 (\vec{v}_1 d\vec{A}_1) \\ &= -v_1 (\cos\theta_1, \sin\theta_1) \, d\dot{m}_1 \end{aligned} \tag{2}$$

where

$$d\dot{m}_1 = \rho v_1 \cos(\theta_1 - \alpha) \, dA_1 . \tag{3}$$

The forces caused by pressure are

$$\begin{aligned} d\vec{F}_{p1} &= p_1 d\vec{A}_1 \\ &= -p_1 (\cos\alpha, \sin\alpha) \, dA_1 . \end{aligned} \tag{4}$$

These force increments have to be summed over all streamtubes. Additionally, they create moments around a moment reference center which is assumed for this calculation to be at the origin of the coordinate system at the tip of the vehicle. The moments are

$$\begin{aligned} d\vec{M} &= \vec{r} \times d\vec{F} \\ &= (x, y) \times (dF_x, dF_y) \\ &= (0, 0, x dF_y - y dF_x) \end{aligned} \tag{5}$$

So the moments caused by x- and y-forces are

$$dM_x = -y \, dF_x \tag{6}$$

$$dM_y = x \, dF_y , \tag{7}$$

respectively. Using the expressions above, the resulting moment increments are

$$dM_{xm1} = yv_1 \cos\theta_1 \, d\dot{m}_1 \tag{8}$$
$$dM_{ym1} = -xv_1 \sin\theta_1 \, d\dot{m}_1 \tag{9}$$
$$dM_{xp1} = yp_1 \cos\alpha \, dA_1 \tag{10}$$
$$dM_{yp1} = -xp_1 \sin\alpha \, dA_1. \tag{11}$$

2. Engine Surface at Body
Since there is no flow across this border of the control volume, only pressure forces are relevant. The outward normal is $\vec{n}_2 = (\sin\alpha, -\cos\alpha)$, so the forces acting on this surface are

$$d\vec{F}_{p2} = p_2(\sin\alpha, -\cos\alpha) \, dA_2. \tag{12}$$

Therefore, the moments are computed as

$$dM_{xp2} = -yp_2 \sin\alpha \, dA_2 \tag{13}$$
$$dM_{yp2} = -xp_2 \cos\alpha \, dA_2. \tag{14}$$

3. Engine Exit Plane
For the engine exhaust, the outcoming flow is naturally parallel to the streamtubes and therefore to the outward normal $\vec{n}_3 = (\cos\alpha, \sin\alpha)$ which leads to the simple expression

$$\vec{v}_3 \, d\vec{A}_3 = v_3 \, dA_3. \tag{15}$$

The forces caused by the momentum flux out of the engine are

$$d\vec{F}_{m3} = v_3(\cos\alpha, \sin\alpha) \, d\dot{m}_3 \tag{16}$$

where

$$d\dot{m}_3 = \rho v_3 \, dA_3. \tag{17}$$

The forces caused by pressure are

$$d\vec{F}_{p3} = p_3(\cos\alpha, \sin\alpha) \, dA_3. \tag{18}$$

The moments can be calculated similarly to the ones at the inlet plane using equations (6) and (7) and the expressions for the forces given above.

4. Engine Surface at Cowl
Like the surface at the body, only pressure forces are relevant. Using the outward normal $\vec{n}_4 = (-\sin\alpha, \cos\alpha)$, the forces and moments are

$$d\vec{F}_{p4} = p_4(-\sin\alpha, \cos\alpha)\, dA_4 \tag{19}$$
$$d\vec{M}_{p4} = p_4(y\sin\alpha, x\cos\alpha)\, dA_4. \tag{20}$$

5. Aftbody Surface
Again, the aftbody is only affected by pressure forces. Denoting the aftbody angle with β measured in the windframe coordinate system, the outward normal is $\vec{n}_5 = (-\sin\beta, -\cos\beta)$ and the forces and moments are

$$d\vec{F}_{p5} = p_5(-\sin\beta, -\cos\beta)\, dA_5 \tag{21}$$
$$d\vec{M}_{p5} = p_5(y\sin\beta, -x\cos\beta)\, dA_5. \tag{22}$$

Total Forces and Moments
When summing the forces and moments over the complete engine module it has to be considered that the difference in momentum and pressure between the inlet and engine exit plane results in a force acting on the fluid. Therefore, the reaction force has to be used when forces acting on the vehicle are to be determined. The pressure forces on the other surfaces act directly on the vehicle. The total forces are then given by

$$\vec{F}_{tot} = -(\vec{F}_{m1} + \vec{F}_{p1} + \vec{F}_{m3} + \vec{F}_{p3}) + \vec{F}_{p2} + \vec{F}_{p4} + \vec{F}_{p5}. \tag{23}$$

Likewise, the total moments are

$$\vec{M}_{tot} = -(\vec{M}_{m1} + \vec{M}_{p1} + \vec{M}_{m3} + \vec{M}_{p3}) + \vec{M}_{p2} + \vec{M}_{p4} + \vec{M}_{p5}. \tag{24}$$

So far, the moments were calculated corresponding to a moment reference center at the origin of the given coordinate system. For the following calculation of the propulsion system database they were transfered to the moment reference center given in [1].

2.3 Propulsion System Database

The HYTHRUST code computes propulsion data for one engine module. The Winged-Cone Configuration utilizes 32 modules around the whole body. For an axisymmetric body at zero angle of attack all modules work under the same conditions and yield an

equal amount of thrust, lift, and pitching moment. This changes when the vehicle is flying at non-zero angles of attack. Compression will be greatest on the underside and gradually decrease when going around the sidewalls to the top. Crossflow components will also influence the flow field considerably and alter the flow entering the sidewall engine inlets.

Since the HYTHRUST code uses an axisymmetric two-dimensional Method of Characteristics procedure on the forebody, this crossflow cannot be tracked and no answer can be given on how the forces will vary for the different engine modules on the sidewalls. Implementing a three-dimensional method for the forebody would have been too time-consuming so an attempt to estimate the force variation along the sidewalls based on experimental results given in [3] and [4] was made. The windtunnel tests described in these papers yielded information about the circumferential pressure distribution around cones at angles of attack at supersonic speeds. Data for the pressure coefficient c_P at the the surface for azimuthal angles of 0° (top), 90° and 180° (bottom) was given and an effort was made to reproduce these data with the HYTHRUST code. The pressure coefficients for top and bottom showed good agreement. However, for an azimuthal angle of 90° our modeling approach resulted in exactly the opposite trend from that given in the papers. The modeling consisted of running the code with free stream conditions $v_\infty^* = v_\infty \cos\alpha$ and introducing an assumed crossflow component $v_\infty \sin\alpha$ at the 90° inlet. Beyond this problem, additional work would have been required to relate the pressure distribution on the forebody to the forces and moments created by the propulsion units.

Since no further information about a reasonably good yet simple estimation could be found a linear approach was chosen. The engine data for the whole vehicle are computed by evaluating the uppermost and lowermost module, since negligible crossflow will occur there, and linearly interpolating for the engine modules in between.

With the propulsion system forces and moments of the vehicle determined by this procedure, the thrust coefficient as defined in [1] is

$$c_T = \frac{\text{thrust}}{q_\infty} \qquad [ft^2] \tag{25}$$

where the dynamic pressure is

$$q_\infty = \frac{1}{2}\rho_\infty v_\infty^2 \tag{26}$$

$$= \frac{1}{2}\gamma p_\infty M_\infty^2. \tag{27}$$

The lift coefficient is

$$c_L = \frac{\text{lift}}{q_\infty S_{ref}} \qquad [-] \tag{28}$$

and the pitching moment coefficient

$$c_M = \frac{\text{pitching moment}}{q_\infty S_{ref} \bar{c}} \qquad [-]. \tag{29}$$

The reference area S_{ref} and reference length $\bar{c}$ are given in [1]. The fuel specific impulse I_{sp} is averaged between the two values for the top and bottom engine module.

The propulsion system database is computed for flight conditions at an altitude of 100000 ft (US Standard Atmosphere 1976) and the following conditions:

Mach numbers:	M = 2, 3, 4, 6, 8, 10, 15, 20, 25
fuel equivalence ratios:	ϕ = 0.25, 0.5, 0.75, 1.0, 1.5, 2.0, 2.5, 3.0, 4.0, 5.0
angles of attack:	$\alpha = 0°, 1°, 2°, 3°, 4°$.

The angle of attack variation is restricted to the condition that there has to be a compression on the forebody for the HYTHRUST code to be applicable. Since the forebody cone half angle is 5°, the 'ramp angle' for an angle of attack of $\alpha = 4°$ is only 1° for the flow on the uppermost engine module which translates into a very weak compression. Since the Winged-Cone Configuration is axisymmetric, the values for negative angles of attack correspond to the positive values where lift and pitching moment reverse sign.

For the zero angle of attack-case data for the thrust coefficient c_T and the fuel specific impulse I_{sp} already exist [1]. Here, an entirely different approach was used to get these data, hence they could not be reproduced by the HYTHRUST code. To overcome this problem the 'percentage change' is measured when deviating from $\alpha = 0°$ and this change is applied on the existing Winged-Cone data for $\alpha = 0°$ to get the angle of attack variation. Using HYTHRUST data, the factor

$$k_T(\alpha) = \frac{c_{T,H}(\alpha) - c_{T,H}(\alpha = 0°)}{c_{T,H}(\alpha = 0°)} \tag{30}$$

is determined and applied on the Winged-Cone data:

$$c_{T,WC}(\alpha) = (1 + k_T(\alpha))\, c_{T,WC}(\alpha = 0°) \tag{31}$$

The fuel specific impulse is adjusted similarly whereas lift and pitching moment coefficients are not changed.

2.4 Results

To get an impression of how close the HYTHRUST code comes in reproducing the data of the Winged-Cone Configuration, a comparison of the thrust coefficients and specific impulses for zero angle of attack and four different Mach numbers representing the whole flight regime is shown in figs. 3, 4, 5 and 6. Phi is the fuel equivalence ratio, c_T is in ft^2 and I_{sp} is in seconds.

The HYTHRUST data for $M = 2$ are considerably lower than the Winged-Cone data which can be explained by the fact that in HYTHRUST a pure scramjet engine is modeled. This type of engine generally does not become effective until the speed increases to Mach numbers above five. This trend can be seen for $M = 8$ in fig. 4 and for $M = 15$ in fig. 5 where the curves for c_T and I_{sp} agree more closely with the Langley Winged-Cone model. For $M = 25$ (fig. 6) HYTHRUST yields higher thrust than the Winged-Cone configuration which is due to the fact that in the HYTHRUST code no boundary layer effects or propulsive drag are considered.

The subsequent figures 7 - 26 give an idea of how vehicle performance is affected by the propulsion system when the angle of attack is changed. For determining the coefficients, the following convention is used: thrust is positive forward and lift is positive upward, both expressed in a windframe system. The pitching moment is positive nose up. As mentioned above, for c_T and I_{sp} the variations due to the angle of attack changes are appplied on the given Winged-Cone data for $\alpha = 0°$ in accordance with equations 30 and 31, whereas the lift and pitching moment coefficients are as given by HYTHRUST. The complete propulsion system database for all Mach numbers, fuel equivalence ratios, and angles of attack is given in the appendix.

Thrust and fuel specific impulse are nearly insensitive to changes in angles of attack. For lower Mach numbers both c_T and I_{sp} slightly decrease for increasing angle of attack, and for higher Mach numbers they may decrease as well as increase marginally depending on the fuel equivalence ratio used.

The lift added to the vehicle by the propulsion system increases for increasing angle of attack. The magnitude of the lift coefficient first increases, then decreases again when the Mach number is varied from 2 to 25. It can be seen especially for $M = 15$ (fig. 20) that there is a certain 'kink' or even a 'jump' for $M = 25$ (fig. 24) in the c_L-curve for small equivalence ratios. This is the result of a simplified modeling of the combustion process as a 'simple' Rayleigh line heat addition. It is assumed that when reaching a certain maximum temperature in the combustion chamber no more fuel is burned and thrust is

Mach	c_{M_α} for basic vehicle	c_{M_α} for prop. system	
		$\phi = 0.5$	$\phi = 1$
4	-0.00175	-0.000119	-0.000091
6	-0.00100	-0.000451	-0.000334
10	0.00050	-0.000550	-0.000515
15	0.00100	-0.000535	-0.000401
20	0.00110	-0.000342	-0.000063
25	0.00110	-0.000174	0.000213

Table 1: c_{M_α} comparison for $\alpha = 1°$

increased by injecting excessive hydrogen. The transition into this fuel-rich environment causes the described effect which is also visible in the graphs of the pitching moment.

The greatest impact on vehicle performance by the propulsion system is in the pitching moment. For small Mach numbers the pitching moment contribution is throughout positive (nose up) (see fig. 9) and increases linearly with fuel equivalence ratio. With increasing speed, c_M becomes negative first for small, and then for all equivalence ratios (see figs. 13 and 17). This trend is reversed when the Mach number is increased further (fig. 21) and for $M = 25$ c_M is positive again for almost all equivalence ratios (fig. 25). Furthermore, the contribution of the propulsion system to the vehicle pitching moment due to angle of attack variations shows a stabilizing tendency. Table 1 gives a comparison of the pitching moment sensitivity to angle of attack changes

$$c_{M_\alpha} = \frac{\partial c_M}{\partial \alpha} \tag{32}$$

for the basic vehicle (derived from fig. 21 in [1]) and for the propulsion system for the equivalence ratios $\phi = 0.5$ and $\phi = 1$ evaluated at $\alpha = 1°$. It can be seen that for Mach numbers around 10 the influence of the propulsion system reaches the same magnitude as the basic vehicle's influence but is reversed in sign and therefore has a stabilizing influence. This effect starts at around M=6 and can still be observed at M=15.

2.5 Conclusions

The investigation shows that the impact of propulsive variations due to angle of attack changes on vehicle performance is not negligible for typical hypersonic vehicles. In this case, it is not so much that thrust is affected but that the pitching moment displays a

significant sensitivity for this type of long and slender vehicle. Even small variations in the forebody conditions can result in considerable changes in the pitching moment which make the vehicle behavior highly unpredictable. This indicates the presence of uncertainty for further control studies.

3 Future Research

During the next reporting period research will concentrate on developing the linear models of the aircraft using the created propulsion sytem model. In this effort we will rely on the results provided by NASA using the POST program as well as investigate the possibility of employing a different code performing the same or a similar task. Furthermore, the uncertainty modeling will be carried out and a paper for the 1993 AIAA Guidance, Navigation and Controls conference will be prepared that will illustrate a control system design based on a robust performance specification.

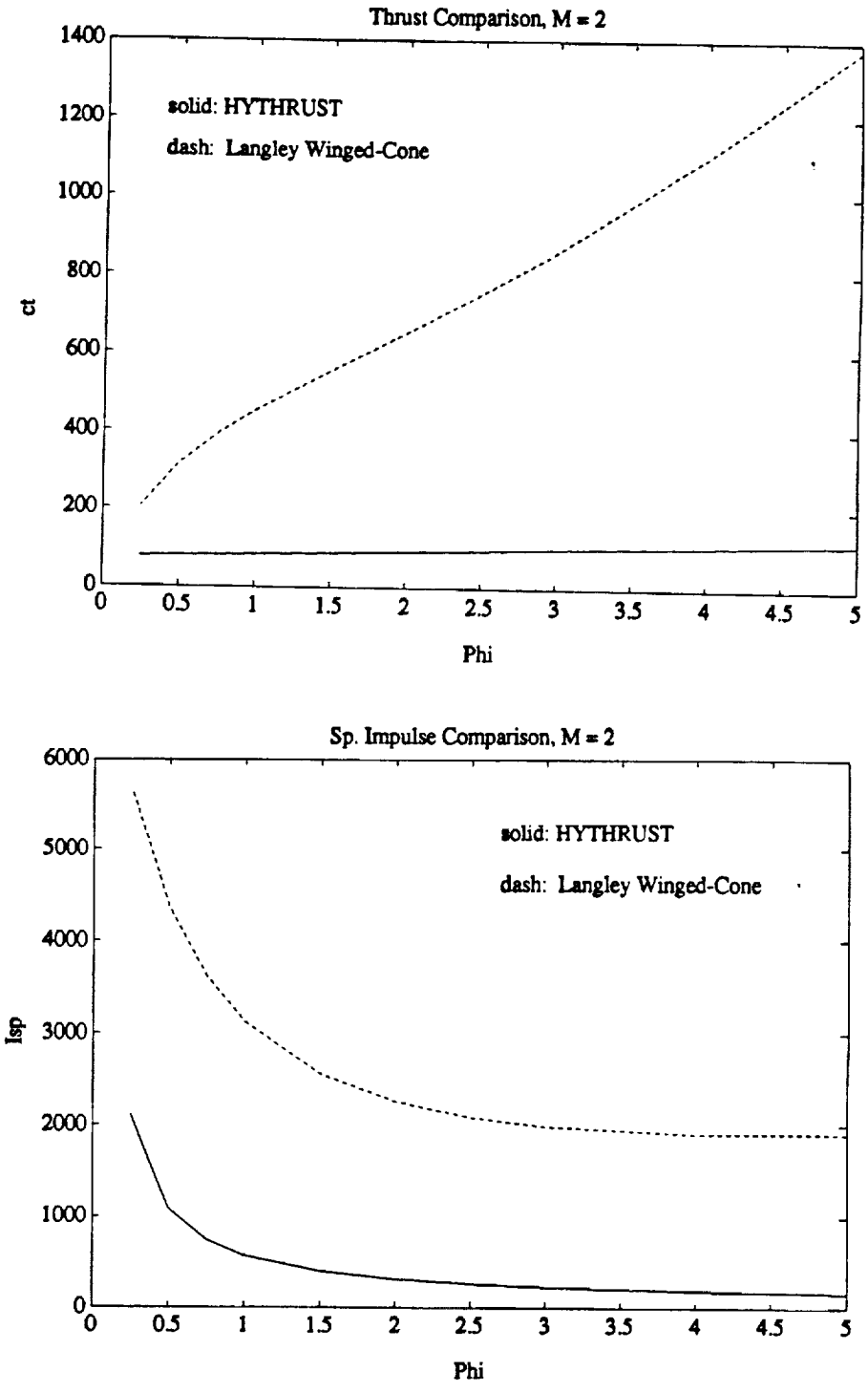

Figure 3: Comparison HYTHRUST and Winged Cone data, $M = 2$

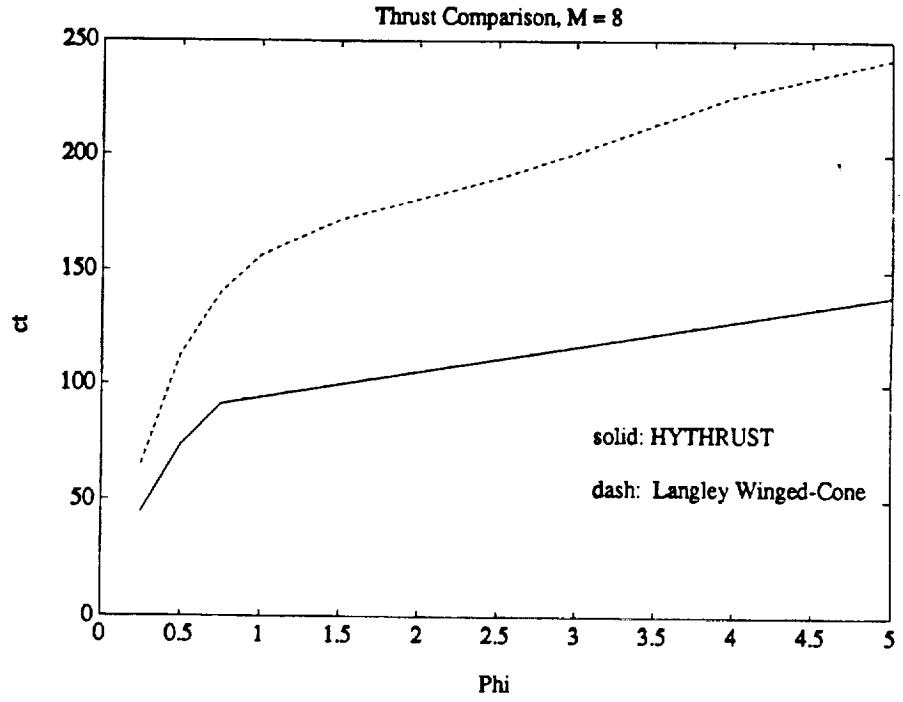

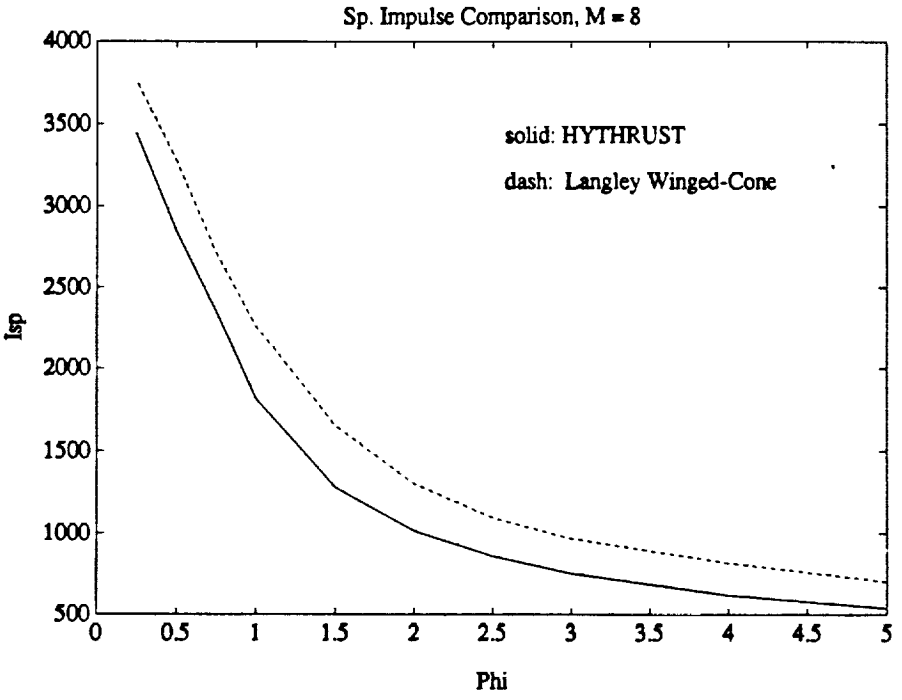

Figure 4: Comparison HYTHRUST and Winged Cone data, $M = 8$

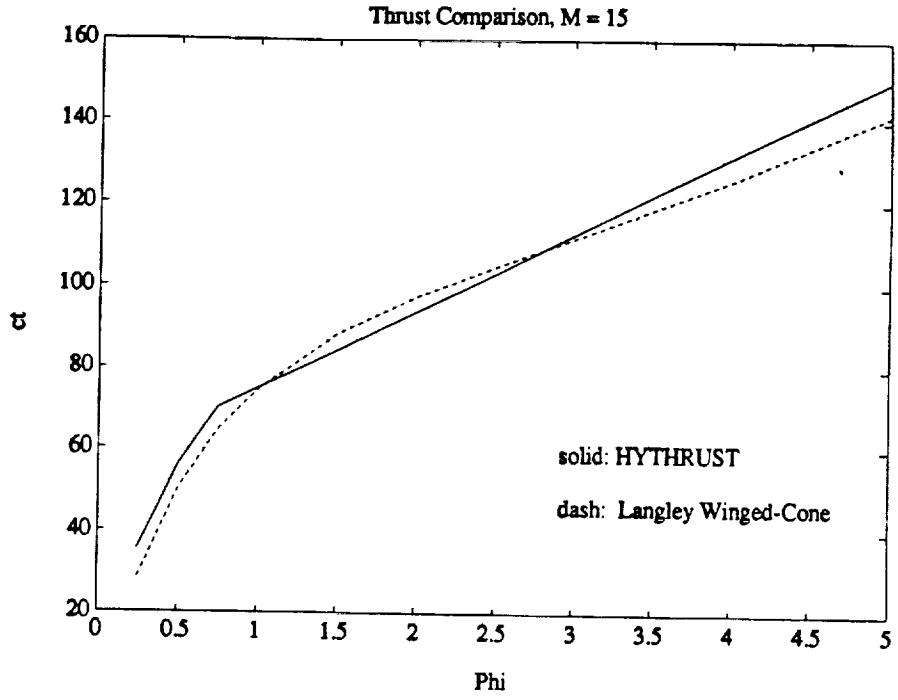

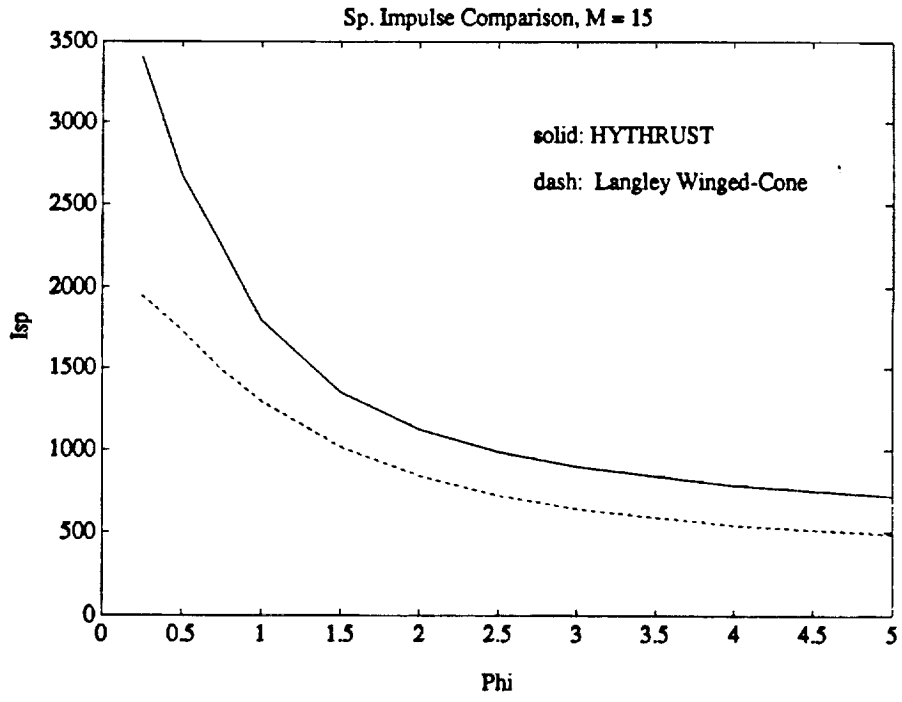

Figure 5: Comparison HYTHRUST and Winged Cone data, $M = 15$

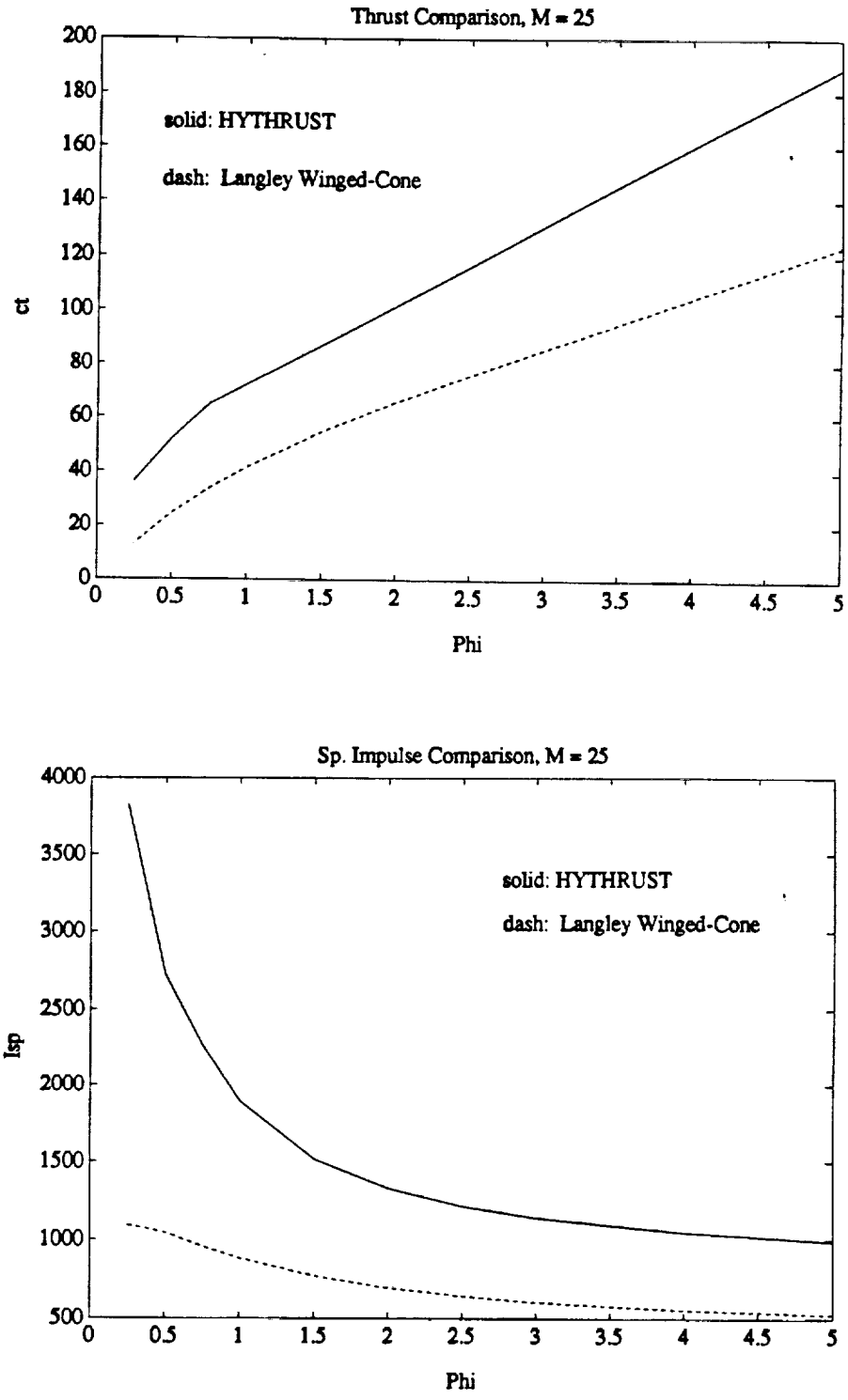

Figure 6: Comparison HYTHRUST and Winged Cone data, $M = 25$

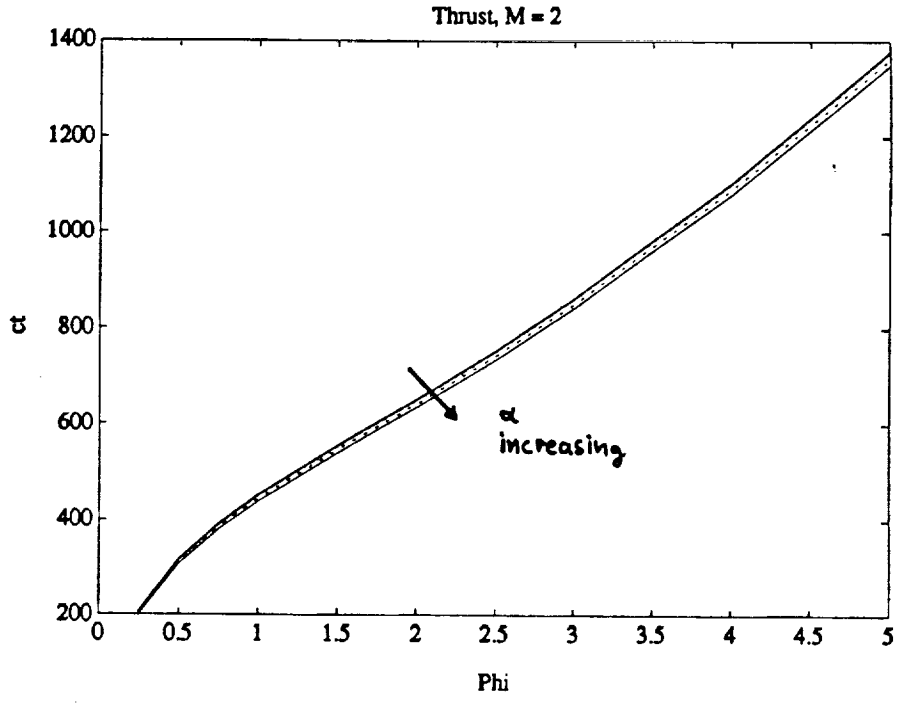

Figure 7: Thrust variation, $M = 2$

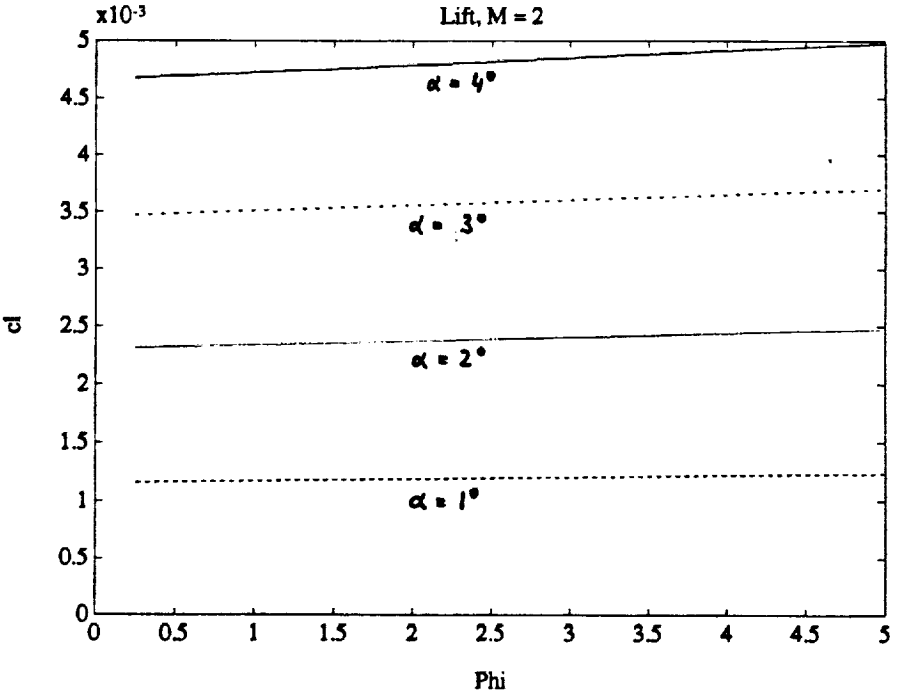

Figure 8: Lift variation, $M = 2$

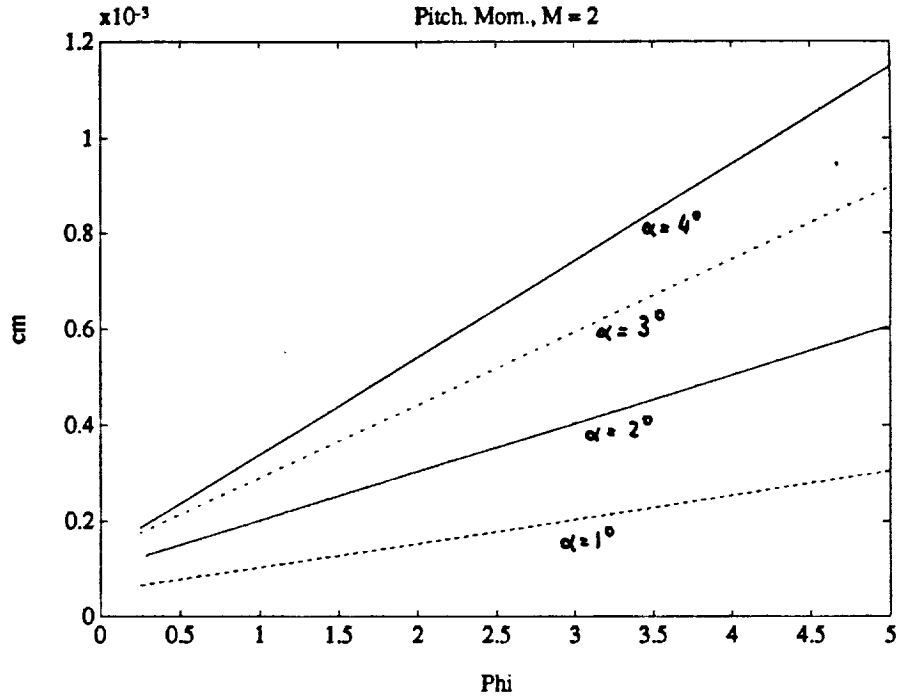

Figure 9: Pitching moment variation, $M = 2$

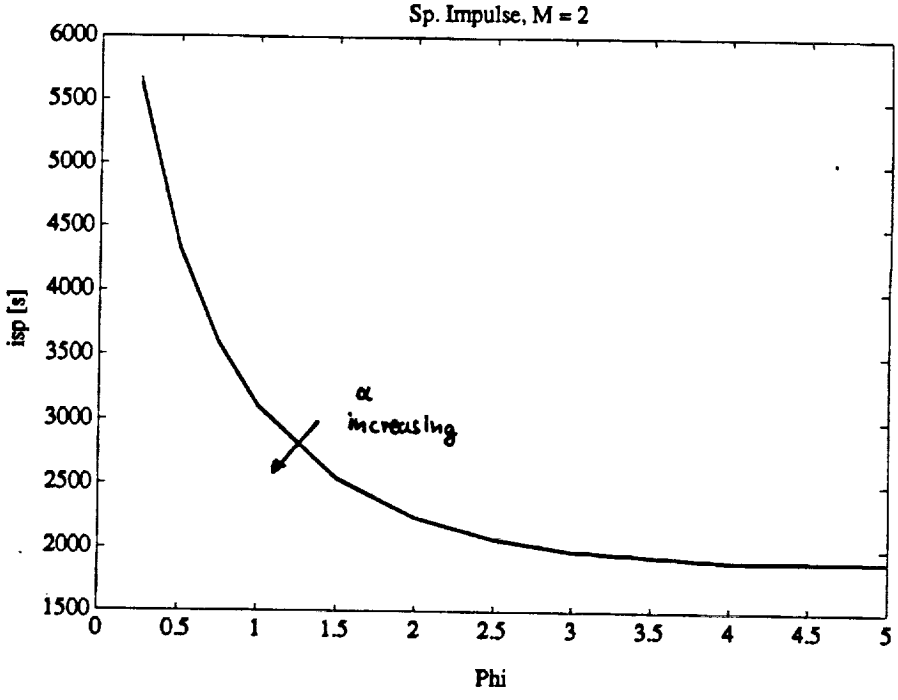

Figure 10: Specific impulse variation, $M = 2$

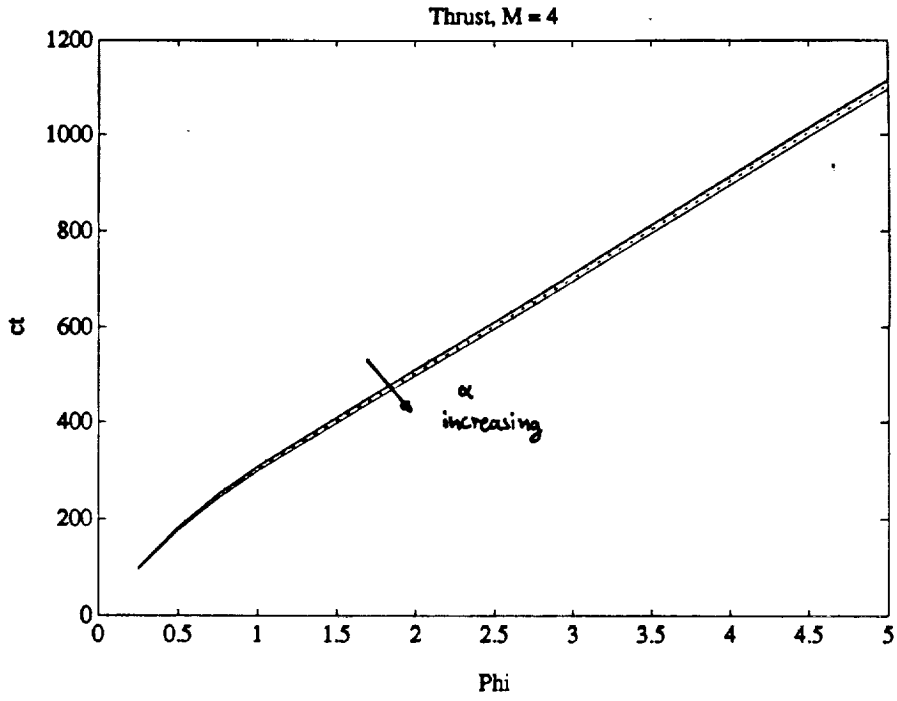

Figure 11: Thrust variation, $M = 4$

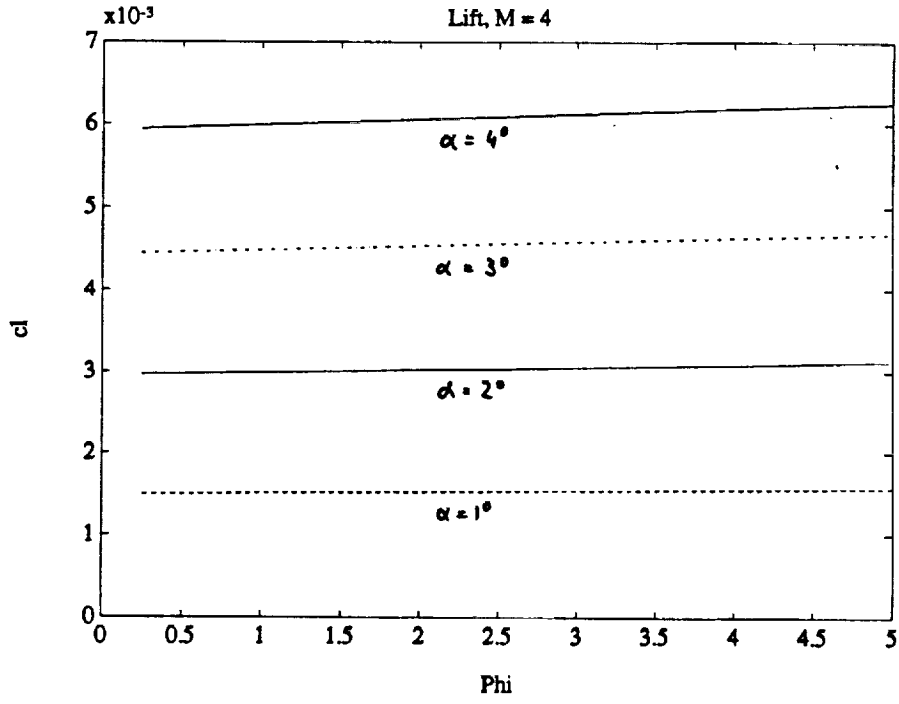

Figure 12: Lift variation, $M = 4$

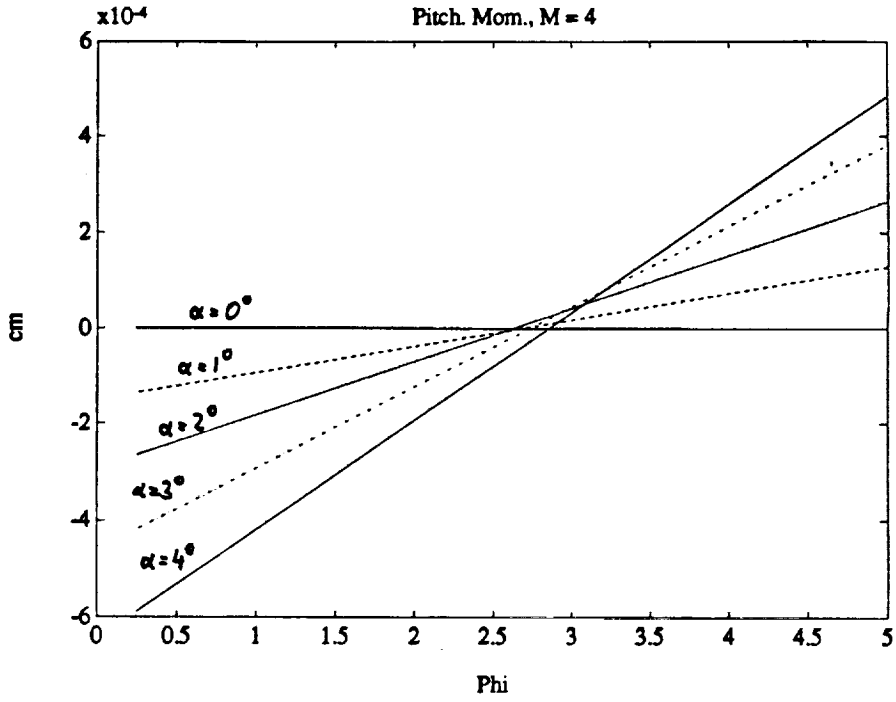

Figure 13: Pitching moment variation, $M = 4$

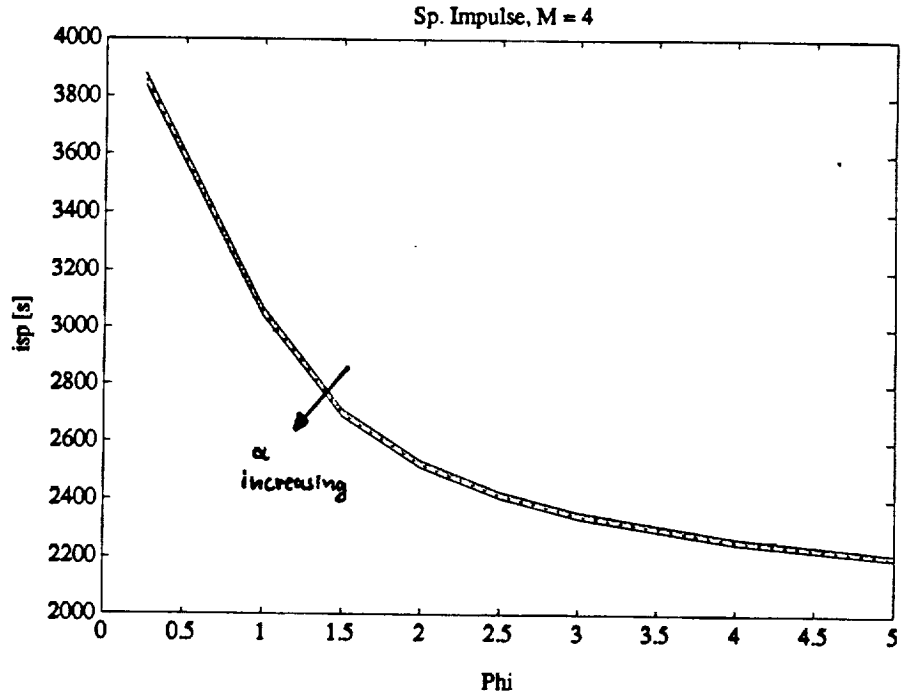

Figure 14: Specific impulse variation, $M = 4$

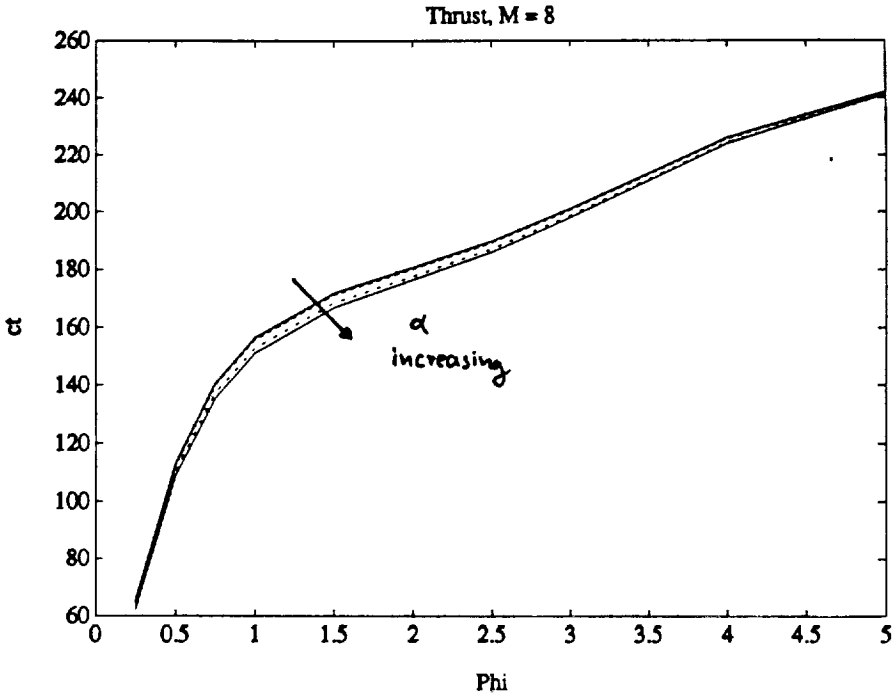

Figure 15: Thrust variation, $M = 8$

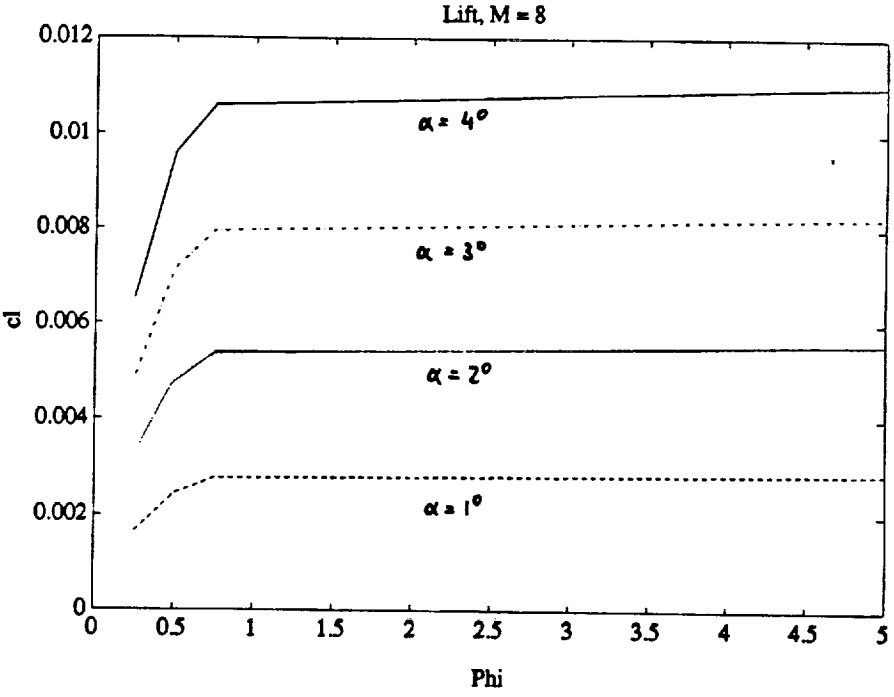

Figure 16: Lift variation, $M = 8$

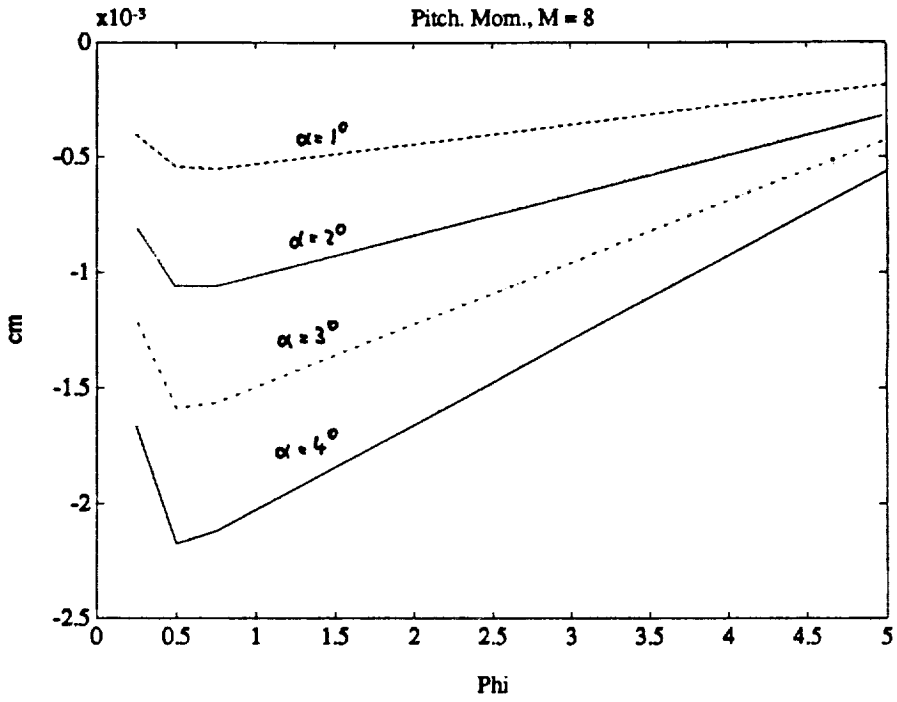

Figure 17: Pitching moment variation, $M = 8$

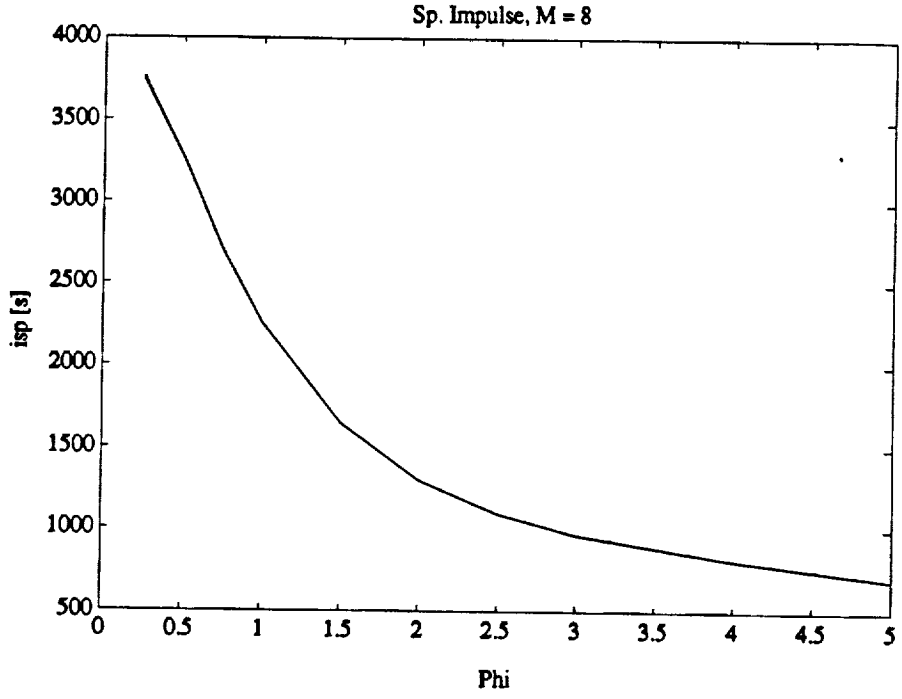

Figure 18: Specific impulse variation, $M = 8$

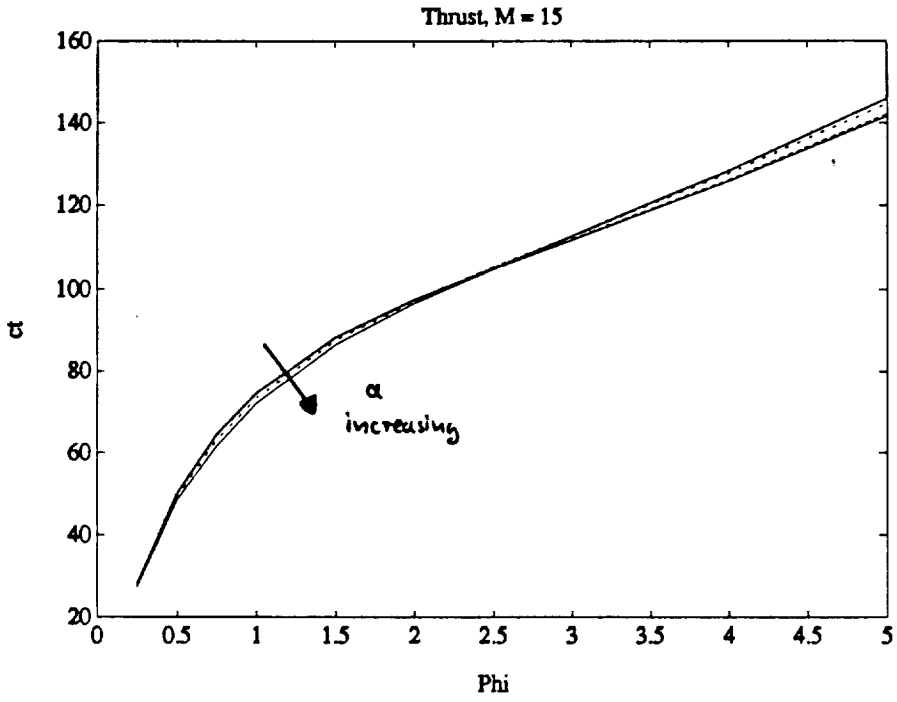

Figure 19: Thrust variation, $M = 15$

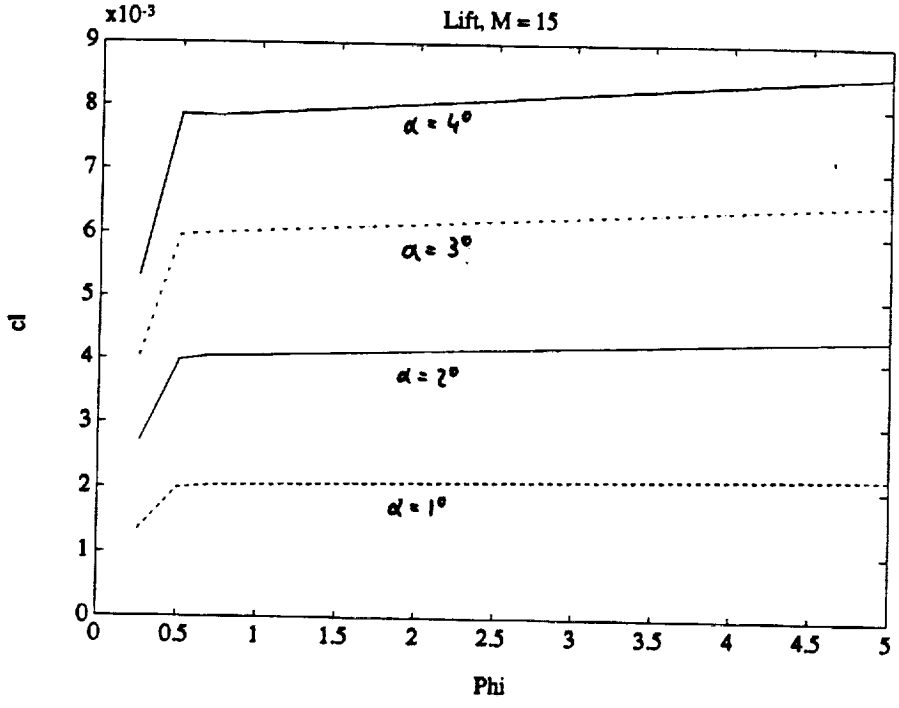

Figure 20: Lift variation, $M = 15$

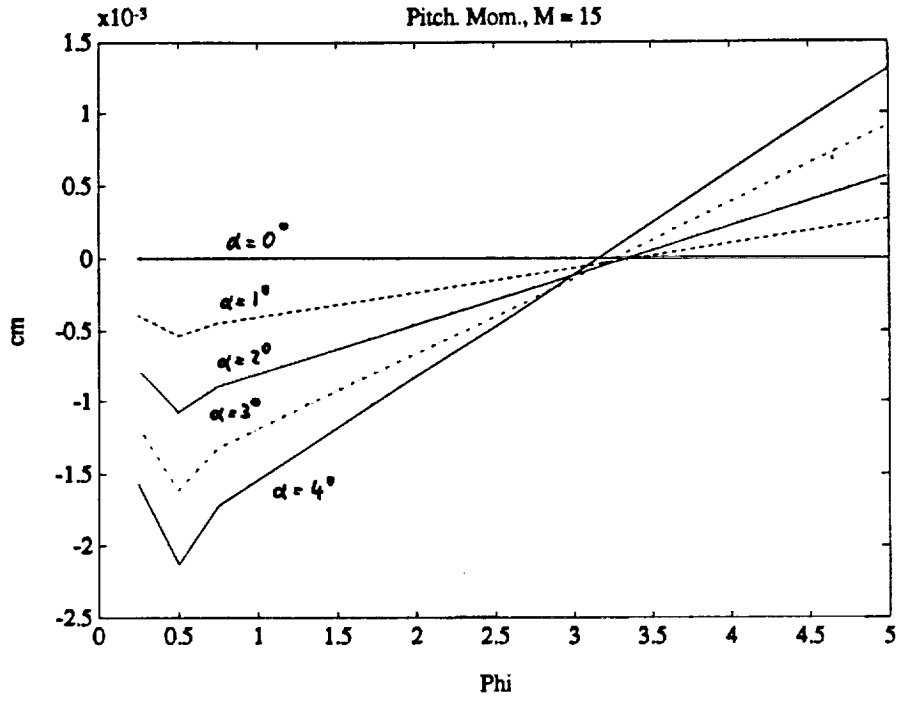

Figure 21: Pitching moment variation, $M = 15$

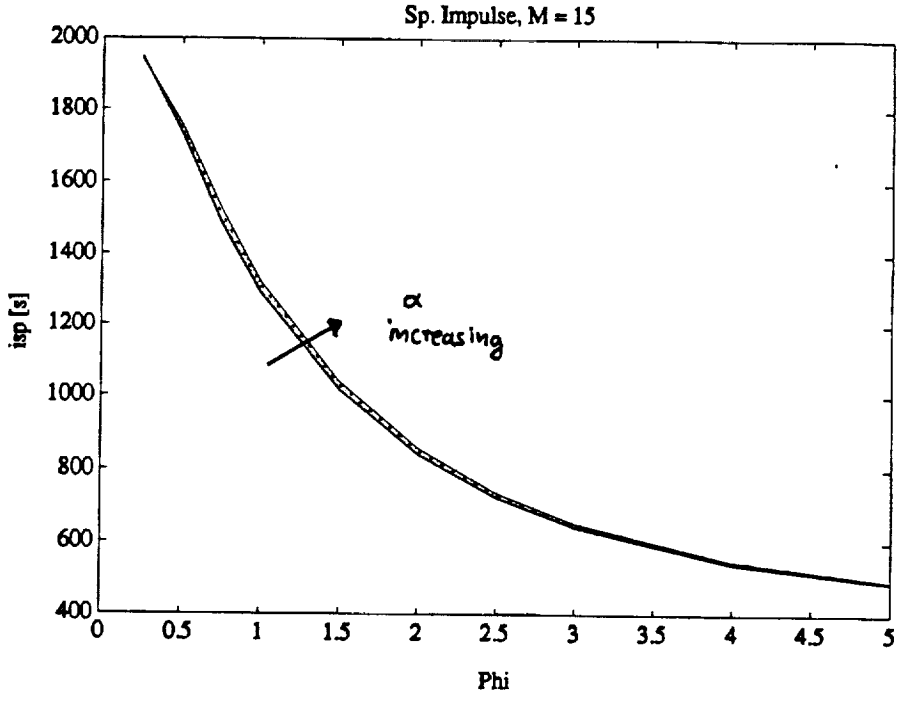

Figure 22: Specific impulse variation, $M = 15$

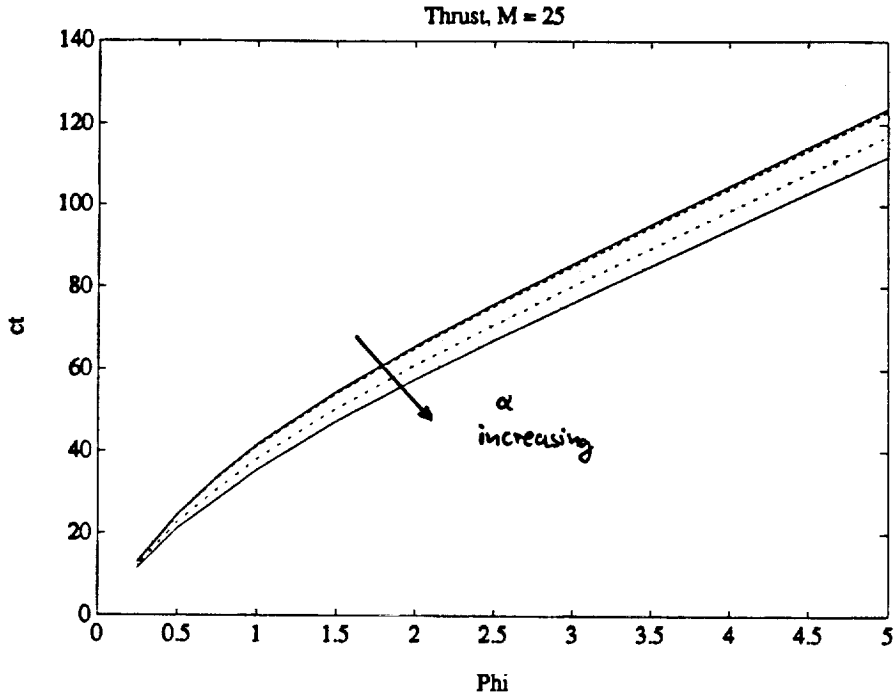

Figure 23: Thrust variation, $M = 25$

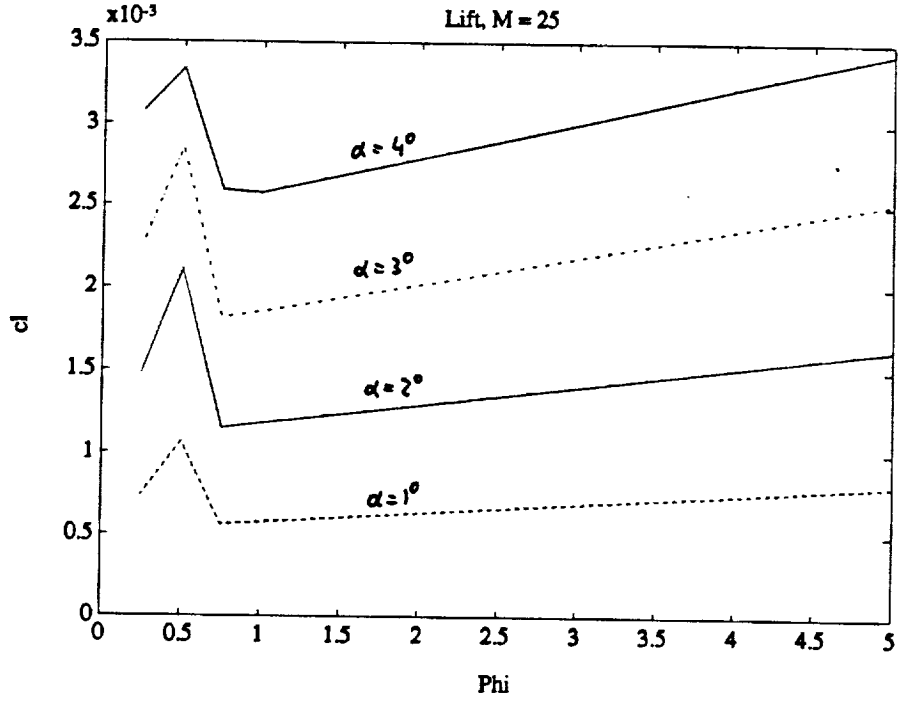

Figure 24: Lift variation, $M = 25$

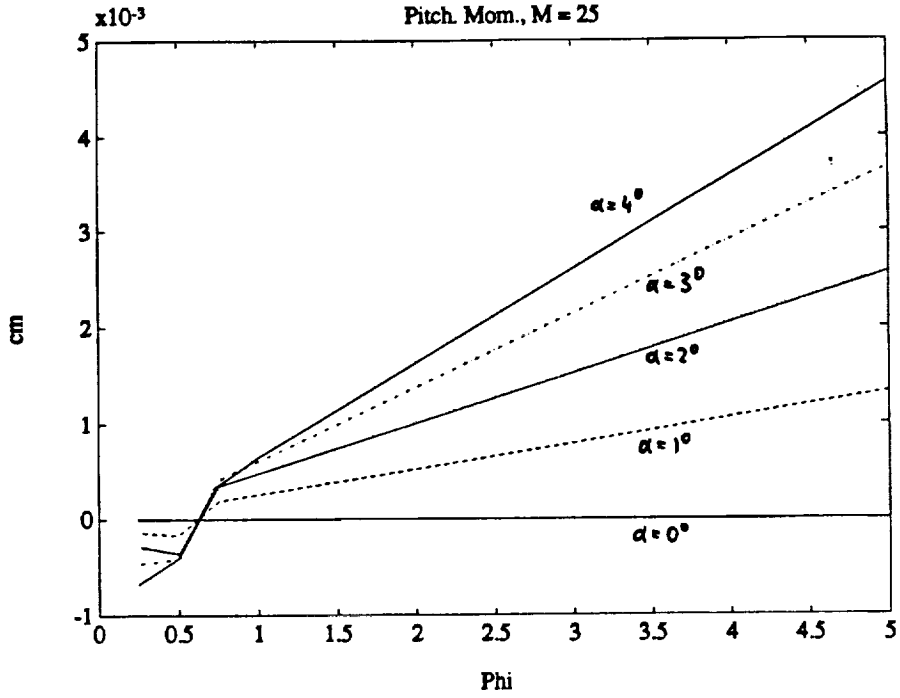

Figure 25: Pitching moment variation, $M = 25$

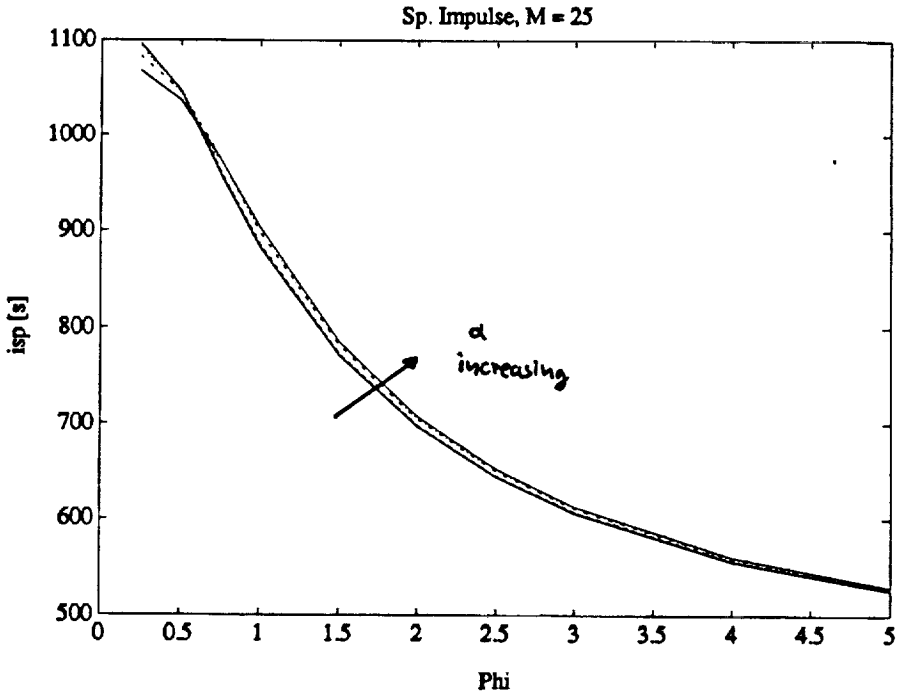

Figure 26: Specific impulse variation, $M = 25$

References

[1] Shaughnessy, J.D., et.al.:
Hypersonic Vehicle Simulation Model: Winged-Cone Configuration
NASA TM 102610, November 1990

[2] Flandro, G.A., Roach, R.L., Buschek, H.:
Dynamic Interactions Between Hypersonic Vehicle Aerodynamics and Propulsion System Performance
Final Report to NASA Langley Research Center, Contract Number NAG-1-1205, July 1992

[3] Rakich, J.V., Cleary, J.W.:
Theoretical and Experimental Study of Supersonic Steady Flow around Inclined Bodies of Revolution
AIAA Journal, Vol. 8, No. 3, pp. 511-518, March 1970

[4] Ferri, A.:
Supersonic Flow around Circular Cones at Angles of Attack
NACA TN 2236, Nov. 1950

Appendix

A.1 Input Data File HYTH.DAT

The input data file used by the HYTHRUST code specifying freestream properties as well as geometrical and combustion data is given below. The expressions on the right hand side of the file represent the names of the variables the values of which are given on the left hand side.

```
 8.     408.6     23.198    0.          AMinf   Tinf   Pinf  alpha
 1.4    1716.                           Gamma   Rgas
 3                                      NPF
 0.       0.       0.                   XF(1)    YF(1)    CF(1)
73.0      6.39      .15658              XF(2)    YF(2)    CF(2)
150.     13.122    .0762                XF(NPF)  YF(NPF)  CF(NPF)
FALSE                                  Lout
2.536    4.5    4.5                    H    XW1   XW2
3.   -3.   -3.    3.                    D1   D1ST  D2   D2ST
150.   14.95   159.   14.95             XCL  YCL   XEX  YEX
5.      0     0.                       XCC  NSTRUT  ALST
1.38    1716.   1.2E9    .96    .0292   G2   RG2   QR   EtaB   FCRIT
.5    0.                               ER    AM
 3                                     NPA
159.     13.122   0.0762                XA(1)    YA(1)    CA(1)
180.      9.796   0.10206               XA(2)    YA(2)    CA(2)
200.      6.63    0.15082               XA(NPA)  YA(NPA)  CA(NPA)
```

A.2 Propulsion database

Here, the complete database for the propulsion system's thrust, lift, and pitching moment contribution including fuel specific impulse data is given for all combinations of Mach number, fuel eqivalence ratio and angle of attack. The expressions in the first block represent the given variables and explain the structure of the database.

```
  M        equ. ratio
alpha      ct        cl          cm        Isp
alpha      ct        cl          cm        Isp
alpha     ..................
```

2.0	0.25			
0.0	205.042	0.000E+00	0.000E+00	5672.40
1.0	204.627	0.116E-02	0.640E-04	5668.14
2.0	203.439	0.232E-02	0.124E-03	5658.67
3.0	201.568	0.347E-02	0.176E-03	5644.48
4.0	198.800	0.467E-02	0.186E-03	5623.08
2.0	0.50			
0.0	315.572	0.000E+00	0.000E+00	4365.00
1.0	314.950	0.116E-02	0.767E-04	4361.78
2.0	313.169	0.232E-02	0.149E-03	4354.61
3.0	310.363	0.348E-02	0.214E-03	4343.85
4.0	306.212	0.469E-02	0.237E-03	4327.63
2.0	0.75			
0.0	391.292	0.000E+00	0.000E+00	3608.30
1.0	390.541	0.117E-02	0.893E-04	3605.68
2.0	388.387	0.233E-02	0.175E-03	3599.85
3.0	384.996	0.350E-02	0.252E-03	3591.07
4.0	379.977	0.471E-02	0.288E-03	3577.87
2.0	1.00			
0.0	451.446	0.000E+00	0.000E+00	3122.20
1.0	450.602	0.117E-02	0.102E-03	3119.97
2.0	448.176	0.234E-02	0.200E-03	3115.00
3.0	444.361	0.351E-02	0.290E-03	3107.51
4.0	438.710	0.472E-02	0.338E-03	3096.25

2.0	1.50			
0.0	553.891	0.000E+00	0.000E+00	2553.90
1.0	552.905	0.118E-02	0.127E-03	2552.14
2.0	550.066	0.236E-02	0.251E-03	2548.18
3.0	545.607	0.353E-02	0.366E-03	2542.21
4.0	538.995	0.475E-02	0.439E-03	2533.25
2.0	2.00			
0.0	651.470	0.000E+00	0.000E+00	2252.90
1.0	650.363	0.119E-02	0.153E-03	2251.39
2.0	647.172	0.237E-02	0.301E-03	2248.00
3.0	642.164	0.356E-02	0.442E-03	2242.85
4.0	634.733	0.479E-02	0.541E-03	2235.15
2.0	2.50			
0.0	753.045	0.000E+00	0.000E+00	2083.20
1.0	751.823	0.120E-02	0.178E-03	2081.84
2.0	748.289	0.239E-02	0.352E-03	2078.79
3.0	742.752	0.358E-02	0.518E-03	2074.13
4.0	734.526	0.482E-02	0.642E-03	2067.18
2.0	3.00			
0.0	861.741	0.000E+00	0.000E+00	1986.60
1.0	860.402	0.120E-02	0.203E-03	1985.34
2.0	856.522	0.240E-02	0.403E-03	1982.49
3.0	850.450	0.360E-02	0.594E-03	1978.15
4.0	841.421	0.485E-02	0.743E-03	1971.67
2.0	4.00			
0.0	1104.097	0.000E+00	0.000E+00	1909.00
1.0	1102.517	0.122E-02	0.254E-03	1907.85
2.0	1097.920	0.244E-02	0.504E-03	1905.23
3.0	1090.741	0.365E-02	0.746E-03	1901.21
4.0	1080.045	0.491E-02	0.946E-03	1895.25
2.0	5.00			
0.0	1379.634	0.000E+00	0.000E+00	1908.30
1.0	1377.805	0.124E-02	0.305E-03	1907.20
2.0	1372.461	0.247E-02	0.605E-03	1904.68
3.0	1364.137	0.370E-02	0.898E-03	1900.80

4.0	1351.711	0.498E-02	0.115E-02	1895.06
3.0	0.25			
0.0	147.409	0.000E+00	0.000E+00	5054.60
1.0	147.104	0.122E-02	-0.712E-04	5051.46
2.0	146.137	0.245E-02	-0.152E-03	5040.61
3.0	144.560	0.366E-02	-0.236E-03	5023.95
4.0	142.334	0.488E-02	-0.344E-03	5001.91
3.0	0.50			
0.0	236.311	0.000E+00	0.000E+00	4051.30
1.0	235.840	0.123E-02	-0.582E-04	4048.83
2.0	234.346	0.246E-02	-0.126E-03	4040.31
3.0	231.909	0.367E-02	-0.197E-03	4027.21
4.0	228.468	0.490E-02	-0.291E-03	4009.87
3.0	0.75			
0.0	303.648	0.000E+00	0.000E+00	3470.60
1.0	303.064	0.123E-02	-0.453E-04	3468.53
2.0	301.212	0.247E-02	-0.996E-04	3461.36
3.0	298.192	0.368E-02	-0.158E-03	3450.34
4.0	293.924	0.491E-02	-0.239E-03	3435.75
3.0	1.00			
0.0	361.339	0.000E+00	0.000E+00	3097.50
1.0	360.669	0.123E-02	-0.323E-04	3095.68
2.0	358.542	0.247E-02	-0.736E-04	3089.41
3.0	355.072	0.370E-02	-0.119E-03	3079.74
4.0	350.166	0.493E-02	-0.187E-03	3066.94
3.0	1.50			
0.0	465.667	0.000E+00	0.000E+00	2661.30
1.0	464.862	0.124E-02	-0.635E-05	2659.79
2.0	462.302	0.249E-02	-0.216E-04	2654.58
3.0	458.127	0.372E-02	-0.405E-04	2646.55
4.0	452.215	0.496E-02	-0.825E-04	2635.91
3.0	2.00			
0.0	566.994	0.000E+00	0.000E+00	2430.20
1.0	566.077	0.125E-02	0.196E-04	2428.86
2.0	563.159	0.251E-02	0.303E-04	2424.26

3.0	558.401	0.374E-02	0.377E-04	2417.15
4.0	551.654	0.499E-02	0.220E-04	2407.72
3.0	2.50			
0.0	670.763	0.000E+00	0.000E+00	2300.00
1.0	669.747	0.126E-02	0.455E-04	2298.77
2.0	666.508	0.252E-02	0.823E-04	2294.55
3.0	661.228	0.377E-02	0.116E-03	2288.01
4.0	653.729	0.502E-02	0.126E-03	2279.33
3.0	3.00			
0.0	778.941	0.000E+00	0.000E+00	2225.80
1.0	777.833	0.127E-02	0.715E-04	2224.64
2.0	774.298	0.254E-02	0.134E-03	2220.67
3.0	768.534	0.379E-02	0.194E-03	2214.52
4.0	760.337	0.506E-02	0.231E-03	2206.33
3.0	4.00			
0.0	1010.740	0.000E+00	0.000E+00	2166.10
1.0	1009.467	0.128E-02	0.123E-03	2165.02
2.0	1005.393	0.257E-02	0.238E-03	2161.36
3.0	998.752	0.384E-02	0.350E-03	2155.66
4.0	989.276	0.512E-02	0.440E-03	2148.07
3.0	5.00			
0.0	1263.073	0.000E+00	0.000E+00	2165.50
1.0	1261.656	0.130E-02	0.175E-03	2164.47
2.0	1257.108	0.260E-02	0.342E-03	2160.97
3.0	1249.697	0.388E-02	0.506E-03	2155.52
4.0	1239.086	0.518E-02	0.649E-03	2148.25
4.0	0.25			
0.0	97.613	0.000E+00	0.000E+00	3877.40
1.0	97.411	0.150E-02	-0.136E-03	3874.75
2.0	96.813	0.296E-02	-0.265E-03	3867.26
3.0	95.732	0.445E-02	-0.419E-03	3854.41
4.0	94.194	0.594E-02	-0.589E-03	3837.19
4.0	0.50			
0.0	181.661	0.000E+00	0.000E+00	3607.90
1.0	181.302	0.150E-02	-0.122E-03	3605.48

2.0	180.237	0.297E-02	-0.237E-03	3598.63
3.0	178.306	0.447E-02	-0.377E-03	3586.88
4.0	175.557	0.595E-02	-0.532E-03	3571.13
4.0	0.75			
0.0	252.147	0.000E+00	0.000E+00	3338.50
1.0	251.670	0.150E-02	-0.108E-03	3336.30
2.0	250.255	0.298E-02	-0.209E-03	3330.06
3.0	247.683	0.448E-02	-0.334E-03	3319.37
4.0	244.014	0.597E-02	-0.476E-03	3305.03
4.0	1.00			
0.0	309.051	0.000E+00	0.000E+00	3069.00
1.0	308.492	0.151E-02	-0.942E-04	3067.01
2.0	306.831	0.299E-02	-0.181E-03	3061.37
3.0	303.802	0.449E-02	-0.292E-03	3051.69
4.0	299.478	0.599E-02	-0.419E-03	3038.72
4.0	1.50			
0.0	409.860	0.000E+00	0.000E+00	2713.30
1.0	409.180	0.152E-02	-0.662E-04	2711.59
2.0	407.159	0.301E-02	-0.126E-03	2706.75
3.0	403.446	0.452E-02	-0.208E-03	2698.46
4.0	398.133	0.602E-02	-0.306E-03	2687.32
4.0	2.00			
0.0	510.648	0.000E+00	0.000E+00	2535.50
1.0	509.870	0.152E-02	-0.383E-04	2533.95
2.0	507.558	0.302E-02	-0.695E-04	2529.55
3.0	503.276	0.454E-02	-0.124E-03	2522.02
4.0	497.132	0.605E-02	-0.193E-03	2511.90
4.0	2.50			
0.0	611.457	0.000E+00	0.000E+00	2428.80
1.0	610.601	0.153E-02	-0.104E-04	2427.35
2.0	608.056	0.304E-02	-0.136E-04	2423.25
3.0	603.304	0.456E-02	-0.393E-04	2416.23
4.0	596.467	0.609E-02	-0.801E-04	2406.78
4.0	3.00			
0.0	712.246	0.000E+00	0.000E+00	2357.60

```
1.0     711.329   0.154E-02   0.175E-04   2356.23
2.0     708.603   0.305E-02   0.424E-04   2352.35
3.0     703.467   0.459E-02   0.450E-04   2345.70
4.0     696.057   0.612E-02   0.329E-04   2336.75

4.0      4.00
0.0     913.843   0.000E+00   0.000E+00   2268.70
1.0     912.849   0.156E-02   0.733E-04   2267.44
2.0     909.890   0.309E-02   0.154E-03   2263.87
3.0     904.204   0.464E-02   0.214E-03   2257.76
4.0     895.947   0.619E-02   0.259E-03   2249.51

4.0      5.00
0.0    1115.440   0.000E+00   0.000E+00   2215.40
1.0    1114.417   0.157E-02   0.129E-03   2214.22
2.0    1111.365   0.312E-02   0.266E-03   2210.87
3.0    1105.368   0.469E-02   0.382E-03   2205.15
4.0    1096.594   0.625E-02   0.485E-03   2197.40

6.0      0.25
0.0      55.631   0.000E+00   0.000E+00   2891.80
1.0      55.453   0.171E-02  -0.360E-03   2889.58
2.0      54.975   0.342E-02  -0.720E-03   2884.36
3.0      54.250   0.510E-02  -0.108E-02   2875.79
4.0      53.265   0.680E-02  -0.147E-02   2865.53

6.0      0.50
0.0     109.213   0.000E+00   0.000E+00   2838.50
1.0     108.941   0.266E-02  -0.458E-03   2836.73
2.0     108.163   0.526E-02  -0.903E-03   2830.83
3.0     106.843   0.750E-02  -0.122E-02   2817.73
4.0     104.887   0.980E-02  -0.160E-02   2797.79

6.0      0.75
0.0     160.746   0.000E+00   0.000E+00   2785.30
1.0     160.291   0.246E-02  -0.352E-03   2783.36
2.0     159.009   0.488E-02  -0.701E-03   2777.34
3.0     157.146   0.722E-02  -0.103E-02   2768.45
4.0     154.755   0.949E-02  -0.136E-02   2759.14

6.0      1.00
```

0.0	210.229	0.000E+00	0.000E+00	2732.00
1.0	209.657	0.246E-02	-0.335E-03	2730.12
2.0	208.045	0.489E-02	-0.667E-03	2724.30
3.0	205.716	0.723E-02	-0.981E-03	2715.69
4.0	202.734	0.951E-02	-0.129E-02	2706.65
6.0	1.50			
0.0	307.229	0.000E+00	0.000E+00	2661.70
1.0	306.453	0.247E-02	-0.301E-03	2659.92
2.0	304.278	0.491E-02	-0.600E-03	2654.39
3.0	301.166	0.726E-02	-0.879E-03	2646.21
4.0	297.204	0.955E-02	-0.116E-02	2637.57
6.0	2.00			
0.0	404.230	0.000E+00	0.000E+00	2626.50
1.0	403.281	0.248E-02	-0.268E-03	2624.78
2.0	400.638	0.493E-02	-0.532E-03	2619.46
3.0	396.896	0.729E-02	-0.777E-03	2611.57
4.0	392.162	0.958E-02	-0.102E-02	2603.20
6.0	2.50			
0.0	501.230	0.000E+00	0.000E+00	2605.50
1.0	500.137	0.249E-02	-0.234E-03	2603.83
2.0	497.107	0.495E-02	-0.465E-03	2598.68
3.0	492.871	0.731E-02	-0.675E-03	2591.01
4.0	487.548	0.962E-02	-0.881E-03	2582.85
6.0	3.00			
0.0	598.230	0.000E+00	0.000E+00	2591.40
1.0	597.017	0.250E-02	-0.201E-03	2589.78
2.0	593.676	0.496E-02	-0.398E-03	2584.76
3.0	589.064	0.734E-02	-0.574E-03	2577.29
4.0	583.314	0.966E-02	-0.743E-03	2569.30
6.0	4.00			
0.0	792.230	0.000E+00	0.000E+00	2573.80
1.0	790.841	0.252E-02	-0.134E-03	2572.25
2.0	787.066	0.500E-02	-0.263E-03	2567.47
3.0	782.010	0.740E-02	-0.370E-03	2560.32
4.0	775.823	0.973E-02	-0.469E-03	2552.61

6.0	5.00			
0.0	986.231	0.000E+00	0.000E+00	2563.30
1.0	984.736	0.253E-02	-0.666E-04	2561.81
2.0	980.740	0.504E-02	-0.129E-03	2557.22
3.0	975.582	0.745E-02	-0.167E-03	2550.34
4.0	969.424	0.981E-02	-0.194E-03	2542.86
8.0	0.25			
0.0	65.041	0.000E+00	0.000E+00	3760.20
1.0	64.787	0.163E-02	-0.405E-03	3757.77
2.0	64.144	0.323E-02	-0.801E-03	3752.24
3.0	63.295	0.483E-02	-0.121E-02	3746.62
4.0	62.197	0.652E-02	-0.167E-02	3738.28
8.0	0.50			
0.0	113.275	0.000E+00	0.000E+00	3274.30
1.0	112.881	0.245E-02	-0.545E-03	3272.89
2.0	111.914	0.480E-02	-0.106E-02	3270.24
3.0	110.672	0.715E-02	-0.159E-02	3267.68
4.0	109.155	0.960E-02	-0.217E-02	3264.41
8.0	0.75			
0.0	140.524	0.000E+00	0.000E+00	2708.00
1.0	140.014	0.277E-02	-0.556E-03	2706.69
2.0	138.764	0.538E-02	-0.106E-02	2704.20
3.0	137.215	0.795E-02	-0.156E-02	2702.66
4.0	135.393	0.106E-01	-0.212E-02	2701.31
8.0	1.00			
0.0	156.161	0.000E+00	0.000E+00	2257.00
1.0	155.624	0.278E-02	-0.534E-03	2255.92
2.0	154.319	0.539E-02	-0.102E-02	2253.83
3.0	152.735	0.797E-02	-0.150E-02	2252.49
4.0	150.903	0.106E-01	-0.203E-02	2251.26
8.0	1.50			
0.0	171.545	0.000E+00	0.146E-08	1652.90
1.0	171.013	0.279E-02	-0.491E-03	1652.12
2.0	169.751	0.542E-02	-0.930E-03	1650.59
3.0	168.287	0.801E-02	-0.136E-02	1649.51
4.0	166.662	0.107E-01	-0.184E-02	1648.48

8.0	2.00			
0.0	180.421	0.000E+00	0.000E+00	1303.80
1.0	179.916	0.280E-02	-0.447E-03	1303.19
2.0	178.749	0.544E-02	-0.842E-03	1301.98
3.0	177.469	0.804E-02	-0.123E-02	1301.07
4.0	176.125	0.107E-01	-0.166E-02	1300.15
8.0	2.50			
0.0	189.713	0.000E+00	0.000E+00	1096.80
1.0	189.234	0.281E-02	-0.403E-03	1096.30
2.0	188.158	0.546E-02	-0.754E-03	1095.27
3.0	187.058	0.807E-02	-0.110E-02	1094.46
4.0	185.988	0.108E-01	-0.148E-02	1093.62
8.0	3.00			
0.0	200.976	0.000E+00	-0.835E-09	968.24
1.0	200.518	0.282E-02	-0.360E-03	967.80
2.0	199.524	0.548E-02	-0.666E-03	966.89
3.0	198.593	0.811E-02	-0.962E-03	966.14
4.0	197.789	0.108E-01	-0.130E-02	965.34
8.0	4.00			
0.0	225.899	0.000E+00	0.000E+00	816.24
1.0	225.481	0.284E-02	-0.273E-03	815.88
2.0	224.646	0.553E-02	-0.490E-03	815.11
3.0	224.058	0.818E-02	-0.694E-03	814.42
4.0	223.796	0.109E-01	-0.930E-03	813.65
8.0	5.00			
0.0	242.087	0.000E+00	0.000E+00	699.78
1.0	241.726	0.286E-02	-0.185E-03	699.47
2.0	241.085	0.557E-02	-0.314E-03	698.81
3.0	240.866	0.825E-02	-0.426E-03	698.18
4.0	241.162	0.110E-01	-0.564E-03	697.46
10.0	0.25			
0.0	49.924	0.000E+00	0.000E+00	3214.10
1.0	49.793	0.153E-02	-0.412E-03	3212.47
2.0	49.413	0.308E-02	-0.840E-03	3209.92
3.0	48.770	0.480E-02	-0.134E-02	3202.70

4.0	48.065	0.647E-02	-0.184E-02	3197.33
10.0	0.50			
0.0	83.253	0.000E+00	0.000E+00	2679.90
1.0	83.062	0.227E-02	-0.548E-03	2680.31
2.0	82.443	0.455E-02	-0.111E-02	2681.10
3.0	81.456	0.706E-02	-0.178E-02	2680.83
4.0	80.456	0.946E-02	-0.241E-02	2684.46
10.0	0.75			
0.0	102.736	0.000E+00	-0.534E-09	2204.60
1.0	102.478	0.251E-02	-0.537E-03	2205.41
2.0	101.653	0.503E-02	-0.108E-02	2207.35
3.0	100.376	0.775E-02	-0.174E-02	2209.50
4.0	99.133	0.103E-01	-0.232E-02	2216.12
10.0	1.00			
0.0	115.382	0.000E+00	0.000E+00	1857.00
1.0	115.127	0.252E-02	-0.509E-03	1857.64
2.0	114.304	0.504E-02	-0.103E-02	1859.14
3.0	113.049	0.777E-02	-0.165E-02	1860.77
4.0	111.892	0.103E-01	-0.221E-02	1865.98
10.0	1.50			
0.0	130.855	0.000E+00	-0.935E-09	1404.00
1.0	130.635	0.253E-02	-0.454E-03	1404.41
2.0	129.913	0.507E-02	-0.917E-03	1405.37
3.0	128.848	0.782E-02	-0.148E-02	1406.37
4.0	128.020	0.104E-01	-0.197E-02	1409.82
10.0	2.00			
0.0	140.495	0.000E+00	0.000E+00	1130.60
1.0	140.323	0.255E-02	-0.399E-03	1130.89
2.0	139.742	0.509E-02	-0.805E-03	1131.54
3.0	138.931	0.786E-02	-0.131E-02	1132.17
4.0	138.490	0.104E-01	-0.174E-02	1134.61
10.0	2.50			
0.0	147.949	0.000E+00	0.000E+00	952.45
1.0	147.827	0.256E-02	-0.344E-03	952.66
2.0	147.394	0.512E-02	-0.694E-03	953.12

3.0	146.844	0.790E-02	-0.114E-02	953.53
4.0	146.790	0.105E-01	-0.150E-02	955.34
10.0	3.00			
0.0	154.732	0.000E+00	0.000E+00	830.11
1.0	154.658	0.257E-02	-0.289E-03	830.27
2.0	154.369	0.515E-02	-0.582E-03	830.60
3.0	154.075	0.794E-02	-0.967E-03	830.87
4.0	154.395	0.106E-01	-0.127E-02	832.25
10.0	4.00			
0.0	168.765	0.000E+00	0.000E+00	679.04
1.0	168.784	0.260E-02	-0.179E-03	679.13
2.0	168.768	0.520E-02	-0.360E-03	679.31
3.0	168.958	0.802E-02	-0.625E-03	679.40
4.0	169.996	0.107E-01	-0.796E-03	680.27
10.0	5.00			
0.0	184.954	0.000E+00	0.000E+00	595.35
1.0	185.062	0.263E-02	-0.696E-04	595.41
2.0	185.309	0.526E-02	-0.137E-03	595.50
3.0	185.968	0.811E-02	-0.284E-03	595.49
4.0	187.714	0.108E-01	-0.327E-03	596.06
15.0	0.25			
0.0	28.204	0.000E+00	0.000E+00	1948.70
1.0	28.191	0.133E-02	-0.392E-03	1947.96
2.0	28.129	0.267E-02	-0.783E-03	1946.36
3.0	27.957	0.401E-02	-0.118E-02	1944.10
4.0	27.562	0.532E-02	-0.157E-02	1941.70
15.0	0.50			
0.0	50.137	0.000E+00	0.237E-09	1732.10
1.0	50.078	0.200E-02	-0.536E-03	1733.77
2.0	49.862	0.398E-02	-0.107E-02	1738.90
3.0	49.381	0.596E-02	-0.161E-02	1746.35
4.0	48.495	0.785E-02	-0.213E-02	1756.53
15.0	0.75			
0.0	64.495	0.000E+00	-0.475E-09	1485.40
1.0	64.369	0.204E-02	-0.447E-03	1488.26

2.0	63.949	0.405E-02	-0.888E-03	1496.75
3.0	63.105	0.601E-02	-0.132E-02	1508.92
4.0	61.709	0.783E-02	-0.172E-02	1524.46
15.0	1.00			
0.0	74.624	0.000E+00	0.000E+00	1289.00
1.0	74.521	0.205E-02	-0.405E-03	1291.31
2.0	74.163	0.407E-02	-0.802E-03	1298.15
3.0	73.392	0.604E-02	-0.119E-02	1307.94
4.0	72.043	0.788E-02	-0.154E-02	1320.43
15.0	1.50			
0.0	88.168	0.000E+00	0.000E+00	1015.30
1.0	88.132	0.207E-02	-0.320E-03	1016.89
2.0	87.957	0.410E-02	-0.630E-03	1021.59
3.0	87.452	0.610E-02	-0.928E-03	1028.29
4.0	86.383	0.796E-02	-0.119E-02	1036.83
15.0	2.00			
0.0	97.358	0.000E+00	0.000E+00	840.85
1.0	97.393	0.209E-02	-0.235E-03	842.01
2.0	97.421	0.414E-02	-0.458E-03	845.45
3.0	97.220	0.616E-02	-0.666E-03	850.34
4.0	96.502	0.804E-02	-0.829E-03	856.54
15.0	2.50			
0.0	104.769	0.000E+00	0.000E+00	723.89
1.0	104.872	0.210E-02	-0.151E-03	724.78
2.0	105.096	0.418E-02	-0.287E-03	727.42
3.0	105.195	0.621E-02	-0.403E-03	731.16
4.0	104.830	0.812E-02	-0.472E-03	735.90
15.0	3.00			
0.0	111.594	0.000E+00	0.475E-09	642.53
1.0	111.762	0.212E-02	-0.662E-04	643.24
2.0	112.173	0.422E-02	-0.115E-03	645.35
3.0	112.557	0.627E-02	-0.140E-03	648.32
4.0	112.530	0.820E-02	-0.116E-03	652.08
15.0	4.00			
0.0	125.637	0.000E+00	0.356E-09	542.54

```
 1.0    125.930   0.216E-02   0.103E-03    543.04
 2.0    126.697   0.430E-02   0.228E-03    544.50
 3.0    127.622   0.639E-02   0.385E-03    546.55
 4.0    128.230   0.836E-02   0.596E-03    549.13

15.0     5.00
 0.0    141.733   0.000E+00   0.000E+00    489.64
 1.0    142.151   0.220E-02   0.272E-03    490.02
 2.0    143.273   0.437E-02   0.572E-03    491.13
 3.0    144.733   0.651E-02   0.910E-03    492.67
 4.0    145.960   0.852E-02   0.131E-02    494.59

20.0     0.25
 0.0     24.548   0.000E+00   0.000E+00   1885.10
 1.0     24.499   0.104E-02  -0.277E-03   1883.26
 2.0     24.335   0.197E-02  -0.514E-03   1879.99
 3.0     23.888   0.300E-02  -0.789E-03   1872.01
 4.0     23.046   0.402E-02  -0.107E-02   1856.84

20.0     0.50
 0.0     44.459   0.000E+00   0.000E+00   1707.00
 1.0     44.319   0.153E-02  -0.368E-03   1708.57
 2.0     43.861   0.293E-02  -0.685E-03   1714.39
 3.0     42.810   0.440E-02  -0.105E-02   1720.75
 4.0     41.036   0.574E-02  -0.137E-02   1725.44

20.0     0.75
 0.0     58.078   0.000E+00   0.000E+00   1486.60
 1.0     57.820   0.129E-02  -0.146E-03   1490.83
 2.0     56.975   0.243E-02  -0.239E-03   1503.27
 3.0     55.210   0.367E-02  -0.396E-03   1519.21
 4.0     52.419   0.482E-02  -0.565E-03   1535.19

20.0     1.00
 0.0     68.082   0.000E+00   0.134E-09   1307.00
 1.0     67.825   0.130E-02  -0.894E-04   1310.38
 2.0     66.967   0.245E-02  -0.126E-03   1320.32
 3.0     65.109   0.370E-02  -0.229E-03   1333.02
 4.0     62.111   0.487E-02  -0.346E-03   1345.69

20.0     1.50
```

0.0	82.204	0.000E+00	0.334E-09	1052.10
1.0	81.981	0.133E-02	0.232E-04	1054.40
2.0	81.195	0.250E-02	0.990E-04	1061.14
3.0	79.353	0.377E-02	0.106E-03	1069.70
4.0	76.252	0.497E-02	0.929E-04	1078.15
20.0	2.00			
0.0	92.411	0.000E+00	-0.134E-09	887.02
1.0	92.234	0.135E-02	0.136E-03	888.68
2.0	91.561	0.255E-02	0.324E-03	893.57
3.0	89.828	0.385E-02	0.441E-03	899.74
4.0	86.779	0.506E-02	0.532E-03	905.75
20.0	2.50			
0.0	100.970	0.000E+00	0.000E+00	775.34
1.0	100.839	0.138E-02	0.249E-03	776.61
2.0	100.282	0.260E-02	0.549E-03	780.34
3.0	98.677	0.392E-02	0.776E-03	785.02
4.0	95.717	0.516E-02	0.970E-03	789.52
20.0	3.00			
0.0	108.965	0.000E+00	0.000E+00	697.28
1.0	108.878	0.140E-02	0.361E-03	698.29
2.0	108.432	0.265E-02	0.774E-03	701.25
3.0	106.947	0.399E-02	0.111E-02	704.95
4.0	104.073	0.526E-02	0.141E-02	708.46
20.0	4.00			
0.0	125.283	0.000E+00	-0.167E-09	601.27
1.0	125.276	0.145E-02	0.587E-03	601.97
2.0	125.029	0.274E-02	0.122E-02	604.02
3.0	123.750	0.414E-02	0.178E-02	606.54
4.0	121.000	0.545E-02	0.229E-02	608.87
20.0	5.00			
0.0	143.513	0.000E+00	0.000E+00	551.01
1.0	143.581	0.150E-02	0.812E-03	551.54
2.0	143.516	0.284E-02	0.167E-02	553.09
3.0	142.402	0.429E-02	0.245E-02	554.96
4.0	139.703	0.565E-02	0.316E-02	556.64

25.0	0.25			
0.0	12.904	0.000E+00	0.000E+00	1096.50
1.0	12.822	0.738E-03	-0.140E-03	1095.23
2.0	12.556	0.148E-02	-0.286E-03	1091.19
3.0	12.083	0.226E-02	-0.461E-03	1082.93
4.0	11.415	0.308E-02	-0.672E-03	1067.45
25.0	0.50			
0.0	24.635	0.000E+00	-0.107E-09	1046.70
1.0	24.451	0.107E-02	-0.170E-03	1047.05
2.0	23.865	0.212E-02	-0.349E-03	1047.84
3.0	22.788	0.285E-02	-0.413E-03	1045.53
4.0	21.241	0.333E-02	-0.401E-03	1036.80
25.0	0.75			
0.0	33.842	0.000E+00	0.000E+00	958.60
1.0	33.529	0.563E-03	0.189E-03	961.18
2.0	32.540	0.115E-02	0.345E-03	968.06
3.0	30.807	0.181E-02	0.411E-03	974.18
4.0	28.457	0.259E-02	0.358E-03	973.49
25.0	1.00			
0.0	41.566	0.000E+00	-0.855E-10	883.00
1.0	41.207	0.577E-03	0.256E-03	885.11
2.0	40.066	0.118E-02	0.476E-03	890.73
3.0	38.116	0.185E-02	0.610E-03	897.72
4.0	35.508	0.257E-02	0.649E-03	903.26
25.0	1.50			
0.0	54.489	0.000E+00	0.192E-09	771.68
1.0	54.067	0.606E-03	0.390E-03	773.18
2.0	52.717	0.123E-02	0.740E-03	777.15
3.0	50.396	0.193E-02	0.993E-03	782.04
4.0	47.294	0.268E-02	0.114E-02	785.80
25.0	2.00			
0.0	65.602	0.000E+00	0.855E-10	696.81
1.0	65.135	0.635E-03	0.524E-03	697.94
2.0	63.634	0.129E-02	0.100E-02	700.92
3.0	61.042	0.202E-02	0.138E-02	704.56
4.0	57.579	0.279E-02	0.163E-02	707.26

25.0	2.50			
0.0	75.820	0.000E+00	0.000E+00	644.28
1.0	75.317	0.663E-03	0.659E-03	645.17
2.0	73.689	0.135E-02	0.127E-02	647.51
3.0	70.868	0.210E-02	0.176E-02	650.33
4.0	67.099	0.290E-02	0.212E-02	652.36
25.0	3.00			
0.0	85.595	0.000E+00	0.000E+00	606.11
1.0	85.059	0.692E-03	0.793E-03	606.83
2.0	83.315	0.140E-02	0.153E-02	608.73
3.0	80.283	0.218E-02	0.214E-02	610.99
4.0	76.234	0.300E-02	0.260E-02	612.55
25.0	4.00			
0.0	104.682	0.000E+00	0.000E+00	555.95
1.0	104.083	0.750E-03	0.106E-02	556.46
2.0	102.116	0.152E-02	0.206E-02	557.80
3.0	98.680	0.235E-02	0.290E-02	559.35
4.0	94.091	0.322E-02	0.358E-02	560.31
25.0	5.00			
0.0	123.848	0.000E+00	0.000E+00	526.19
1.0	123.185	0.807E-03	0.133E-02	526.58
2.0	120.994	0.163E-02	0.258E-02	527.58
3.0	117.151	0.252E-02	0.367E-02	528.70
4.0	112.019	0.344E-02	0.456E-02	529.31